

The *Drosophila* epidermal growth factor receptor pathway regulates Hedgehog signalling and cytoneme behaviour

Received: 25 January 2023

Accepted: 12 February 2025

Published online: 26 February 2025



Vasiliki S. Lalioti^{1,4}, Ana-Citlali Gradilla^{1,2,4}, Carlos Jiménez-Jiménez¹, Clara Fernández-Pardo¹, David Sánchez-Hernández¹, Adrián Aguirre-Tamaral^{1,3}, Irene Sánchez-Platero¹, Sheila Jordán-Álvarez¹, James G. Wakefield² & Isabel Guerrero¹✉

During *Drosophila* epithelial development, dynamic signalling filopodia (cytonemes) establish direct contacts between distant cells to facilitate the formation of the Hedgehog signalling gradient. However, not much is known about how cytonemes are regulated. In this study, we show that cytoneme dynamics and Hedgehog signalling in the *Drosophila* epithelia depend on the Epidermal Growth Factor pathway and on its downstream effector Ras1. We describe that EGFR/Ras1 pathway is required to maintain in the wing disc epithelium the basal plasma membrane levels of Interference Hedgehog (Ihog), a critical Hh co-receptor and adhesion protein. In addition, our data demonstrate that filamin A or Cheerio in *Drosophila*, responds to both Ihog and EGFR pathway and recruited to the basal site of the plasma membrane. This recruitment contributes to Ihog's role in stabilizing cytonemes.

Signalling-specialized filopodia, or cytonemes, are cell protrusions that enable direct cell-to-cell communication at a distance, both within tissues as well as between associated but physically separated tissues (reviewed in ref. 1). Cytonemes are dynamic structures that regulate Hedgehog (Hh), Wnt, Fibroblast Growth Factor (FGF), Bone morphogenetic protein (BMP), Epidermal Growth Factor (EGF) and Notch signalling (reviewed^{2–4}). Cytonemes are fundamental structures for Hh signalling during *Drosophila* development, regulating restricted signalling during stem cell maintenance⁵ and Hh-graded distribution in the wing disc and abdominal epithelia^{6–8}. Cytoneme-mediated Sonic-Hh signalling has also been found during limb development in chicken limb buds⁹, limb regeneration in axolotls¹⁰, neural tube development in zebra fish¹¹ and in mouse^{12,13}. In these contexts, cytonemes are engaged in direct cellular membrane-to-membrane contact, either between two meeting cytonemes or between cytonemes and cell body membranes (reviewed in ref. 3). In the case of Hh signalling in *Drosophila* polarized epithelia, a synapse-like contact occurs between basally located cytonemes emanating from Hh producing and receiving cells^{7,8,14,15}.

Structurally, cytonemes are thin cytoplasmic protrusions filled with parallel bundles of actin filaments that elongate pushing the membrane outwards². The initiation phase of filopodia formation begins with a cytoplasmic influx and the generation of a membrane bud; then, filopodia arise during an elongation phase where actin filaments extend (reviewed in ref. 16). These processes are dependent on the activation of small GTPases Cdc42¹⁷ and actin nucleation factors such as formin Dia2^{18,19} or suppressor of cyclic AMP receptor (SCAR). All these components have been shown to disrupt cytoneme behaviour and Hh signalling in the *Drosophila* wing disc^{6–8}, evidencing the shared cellular machinery between cytonemes and other filopodia.

We have previously proposed that cytoneme dynamics are key for the formation of the Hh gradient¹⁴. In contrast to other pathways (Roy et al.²⁰), it seems that cytoneme formation does not depend on Hh signalling⁸. However, over-expression of the Hh co-receptor and adhesion protein Ihog in the wing disc stabilizes cytoneme dynamics^{6,8,21}. Ihog is a type I transmembrane protein, with four immunoglobulin (Ig) and two fibronectin type III (FNIII) extracellular

¹Centro de Biología Molecular Severo Ochoa, Consejo Superior de Investigaciones Científicas-Universidad Autónoma de Madrid, Madrid, Spain. ²Living Systems Institute/Department of Biosciences, University of Exeter, Exeter, UK. ³Present address: Department of Biology, University of Graz, Graz, Austria.

⁴These authors contributed equally: Vasiliki S. Lalioti, Ana-Citlali Gradilla. ✉e-mail: iguerrero@cblm.csic.es

domains and an intracellular domain²². The ability to stabilize cytonemes is mediated through the extracellular FNIII domains of Ihog. Thus far, cytoneme stabilization by Ihog is known to rely on the balance between homophilic Ihog-Ihog interactions and heterophilic interactions of the extracellular region of Ihog with glypicans, specifically Dally and Dally-like^{21,23,24}. However, it is still unclear how Hh cytonemes are initiated and how their dynamics are regulated in addition to Ihog.

EGF is a well-known protrusion promoter in mammalian cells^{25–29}. Conversely, EGFR inhibition disrupts protrusion-dependent cell behaviours such as cell migration, including during metastasis^{25,30}. Furthermore, EGFR activation has also been shown to have a rapid effect on the formation of filopodia during axon development³¹. Observations in *Drosophila* of retrograde transport of active EGFR on filopodia led to the suggestion that these filopodia extended towards an EGF source³², implying that the pathway could be key for initiation and/or dynamics of cell membrane protrusions. In addition, activated tyrosine kinase receptors such as EGFR are linked to intracellular transducers by the GTPase Ras family, which is also known to affect filopodia formation³³. As in mammalian cells, overexpression of an oncogenic activated form of Ras1 (Ras^{V12}) or the constitutive active form of EGFR (EGFR^{CA}) in groups of cells in the fly wing disc leads to hyperplastic growth (reviewed in ref. 34).

The work described here shows that Hh cytoneme dynamics and Hh signalling also depend on EGFR signalling. We have observed that the membrane presence of Ihog in the basal side of the disc epithelium relies on EGFR signalling and its downstream GTPase Ras1. On the other hand, Ihog interacts with actin cytoskeleton regulators, and these interactions are EGF-dependent, linking the Hh pathway to known general regulators of filopodia. Our findings suggest that ectopic expression of Ihog stabilizes cytonemes by directing the actin cross-linker Cheerio (Cher, the ortholog of filamin A) to focal points on the plasma membrane.

Results

EGFR pathway modulates cytoneme dynamics and Hh signalling

Given the extensively reported relationship between EGFR signalling and cytoskeletal dynamics^{25–29}, we have investigated whether the EGFR signalling in *Drosophila* affects cytoneme dynamics in the wing disc and abdominal histoblast nests. Due to their fragility, cytonemes are rarely preserved in fixed tissues. Despite these adverse conditions for their visualization, overexpression of EGFR^{CA} or the Ras^{V12}, together with the actin marker GMA^{GFP} in the posterior (P) compartment of wing imaginal discs, resulted in an increase in the number and length of GMA^{GFP} labelled cytonemes per disc compared with control expressing only GMA^{GFP} (Fig. 1A, and quantifications in Fig. 1B) (Supplementary Fig. 1 shows the efficacy of the tools used in these studies for both gain and loss of function of EGFR signalling).

We have previously postulated that cytoneme dynamics are key for the establishment of Hh signalling gradient¹⁴; Building on this we then investigated whether Hh signalling itself could be affected by the EGFR signalling. We expressed RNAi against EGFR or EGFR^{CA} in the dorsal compartment of the wing disc using *ap.Gal4* driver. Our comparisons of the ventral and dorsal disc compartments showed a decrease of Hh signalling (Supplementary Fig. 2A, B) in response to EGFR inhibition and an increase in response to its activation (Supplementary Fig. 2A, C).

To analyse if the observed effect on Hh signalling in the wing disc corresponded to defects on the Hh-receiving or Hh-producing cells, we expressed EGFR^{RNAi} or Ras1^{RNAi} in the anterior-ventral quadrant (using the genetic combination *LexA-Op.Gal80*; *ap.LexA.ptc.Gal4*; *tub.Gal80^{ts}*) to exclusively manipulate the Hh receiving cells, or in the posterior-ventral quadrant (using *LexA-Op.Gal80*; *ap.LexA*; *hh.Gal4 tub.Gal80^{ts}*) to solely affect the producing cells (see representative schemes of the expression domains on the left side of the Fig. 1C and

Supplementary Fig. 2D). With these expression systems, we can maintain the dorsal side of the disc as an internal wild-type control and analyse and quantify the responses of the high threshold target Patched (Ptc) and the low threshold target Cubitus interruptus (Ci) after expression of EGFR^{RNAi} or Ras1^{RNAi}. Using these drivers, we found that Hh signalling was downregulated in response to transient EGFR or Ras1 inhibition in the A (Fig. 1C–C2, D–D2 and c1 c2 and d1 d2 for quantifications) or in the P compartment (Supplementary Fig. 2D, E and d1, d2 and e1, e2 for quantifications). This data demonstrates that EGFR/Ras1 pathway modulates Hh signalling pathway and that this effect affects both Hh-producing and Hh-receiving cells.

Our previous experience analysing cytoneme dynamics indicated that in vivo cytonemes were better visualized in developing abdominal histoblast nests than in wing imaginal discs⁶. We, therefore, analysed by life imaging in this system if EGFR inhibition could affect cytoneme dynamics by co-expressing GMA^{GFP} in the P compartment of the abdominal histoblast nests. We compared cytonemes from cells co-expressing EGFR^{RNAi} with controls and found that GMA^{GFP} marked cytonemes from cells with normal EGFR were longer lived (12 min) than cytonemes from cells lacking EGFR (average of 9.2 min) (Fig. 2A for Supplementary Movie 1 and 2B for the corresponding violin plots). Since the EGFR pathway is known to be required for histoblast proliferation during the *Drosophila* pupal stage, and activation of the EGFR/Ras1 signalling pathway is detected by elevated levels of phospho-ERK staining in histoblasts³⁵, these results show that EGF signalling has an impact on normal cytoneme dynamics.

EGFR pathway modulates the stabilizing effect of Ihog on cytonemes

In a previous study⁸, we reported that the overexpression of the Hh co-receptor Ihog resulted in the stabilization (immobilization of dynamics) of cytonemes, both in abdominal histoblasts and in wing imaginal discs. Here, we first investigated whether Ihog-stabilised cytonemes could also be modified by EGFR signalling in the abdominal histoblasts. We examined Ihog overexpressed cytonemes by life imaging under EGFR inhibition and observed significant differences in cytoneme behaviour. Specifically, cytonemes extending from histoblasts expressing Ihog and the actin marker GMA^{GFP} exhibited an average lifetime of 29.3 min. In contrast, cytonemes from cells expressing only GMA^{GFP} or co-expressing Ihog^{RFP} and EGFR^{RNAi} displayed similar shorter lifetimes, measuring 11.9 min and 12.6 min, respectively (Fig. 2C for Supplementary Movie 2 and D for violin plots quantifications). These results also indicate a role for the EGFR pathway in promoting Ihog-mediated cytoneme stabilization.

Following this finding, we co-expressed Ihog^{RFP} together with the EGFR modulating reagents in the P compartment of wing discs (Fig. 3A–D) (see disc models for expression domains on the left-hand side of Fig. 3A and G). In this setup, we measured and quantified the number and length of cytonemes extending from the P/A compartment border towards the Hh receiving area in the A compartment (Fig. 3E, F). Stabilized cytonemes were barely observed in the presence of EGFR^{RNAi} (Fig. 3B compare panels B with A). The few cytonemes observed were abnormally short (~5 µm), in contrast to cytonemes that extended from cells with normal EGFR (up to 32 µm) (Fig. 3F). Co-expression of a dominant negative EGFR (EGFR^{DN}) with Ihog^{RFP} also resulted in a decrease in cytoneme number (Fig. 3C, compare panels C with A, and quantifications in Fig. 3E). Consistent with the idea that EGF signalling could be important for cytoneme dynamics, overexpression of EGFR^{CA} slightly increased both number and length of Ihog-stabilized cytonemes in fixed tissues (Fig. 3, compare panels D with A). Some cytonemes from cells with ectopically activated EGFR signalling extended further than controls but the average length was still similar (Fig. 3E, F). In a concurrent set of experiments, we quantified the cytonemes stabilized by Ihog^{RFP}, which express Ras1^{RNAi} or the dominant negative form of Ras1 (Ras1^{DN}) in the P/A compartment. The effect

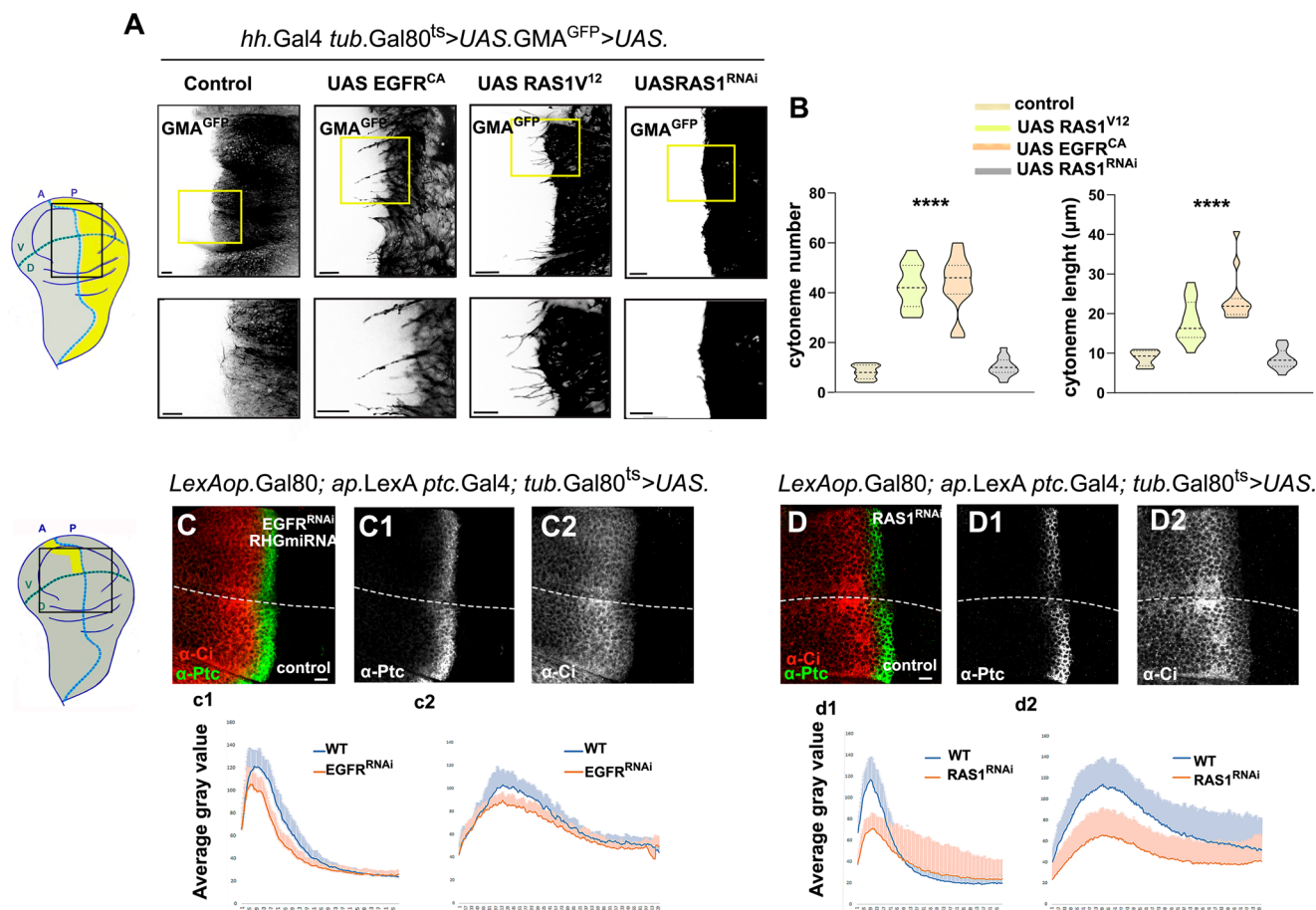


Fig. 1 | EGFR/Ras1 pathway controls cytoneme stability and Hh signalling.

A Cytonemes visualized by ectopic expression in the P compartment of either UAS.GMA^{GFP} alone or together with either UAS.EGFR^{CA} or Ras1^{V12} or Ras1^{RNAi} for 24 h in *hh.Gal4,tub.Gal80^{ts}>UAS.RHGmiRNA* wing discs. Scale bars = 10 μm. Enlargements of confocal images in the selected areas (light brown windows) are shown underneath. Scale bars = 5 μm. **B** The quantifications of the number and length of cytonemes in the same experimental conditions as above were analysed by ANOVA test (p -value < 0.0001). The lines at the violins are presented mean value ± SD. Responses of the Hh pathway after the induction of EGFR^{RNAi} (**C**) and of the Ras1^{RNAi} (**D**) for 24 h in the Hh receiving cells of the anterior and ventral compartments of an *ap.LexA tub.Gal80;ap.LexA ptc.Gal4;tub.Gal80^{ts}>UAS.RHGmiRNA* wing discs, using

the dorsal side of the disc as internal control (the scheme at the left side represents the expression domains). Gradient lengths measuring the response of the Hh target Ptc (green) y Ci (Red) with specific antibody staining. Note the decrease of the Hh signalling gradient. Scale bars = 10 μm. **c1, c2, d1, d2**. Fluorescence quantifications of the dorsal (control, blue) and ventral compartments (experimental conditions, red). Statistical analysis was performed on a set of 10-15 discs using GraphPad, specifically employing the ANOVA test (p < 0.0001). The blue lines in the gradient models represent the activation of the Hh targets Ptc and Ci in wild type and the orange lines represent the activation of Ptc and Ci in EGFR and Ras1 mutant conditions. The solid lines represent the minimum and the shaded areas the variability. Source data are provided as a Source Data file.

of RNAi was very similar to that of the Ras1^{DN}, in terms of the significant decrease in both number and length of cytonemes (Fig. 3G–K for quantifications). These results suggest that not only the EGF receptor but also the downstream Ras1 promotes Ihog-mediated stabilization of cytonemes.

Similar results were observed for cytonemes in clones of cells expressing Ihog^{RFP} in discs in which EGFR was inhibited in the dorsal but not in the ventral compartment (see disc model for expression domains on the left-hand side of Fig. 3L). We did not observe cytonemes extending from cells lacking EGFR activity (dorsal compartment of Fig. 3N), but they were visible when clones were in areas of wild-type EGFR activity (Fig. 3L and ventral part of Fig. 3N). These results are consistent with the previous observations that the role of the EGF pathway influences the dynamics of both normal and Ihog-stabilized cytonemes. Interestingly, we also noted that comparisons of clones in wild type or EGFR mutated regions revealed that the levels of Ihog^{RFP} at plasma membranes were reduced under EGFR^{RNAi} expression (Fig. 3L, M compared with the dorsal compartment of Fig. 3N, O).

Noticing this decrease on Ihog levels in mutant conditions for EGFR, we went on and analyse ectopic Ihog^{RFP} levels under different

conditions of loss or gain of function of the EGFR/Ras1 pathway. We observed upregulation of Ihog^{RFP} levels when coexpressing Ihog^{RFP} with either EGFR^{CA} or Ras1^{V12} and downregulation of Ihog^{RFP} levels when coexpressing Ihog^{RFP} with either EGFR^{RNAi}, Ras1^{RNAi} or Ras1^{DN} (Fig. 3P).

The ligands Spitz and Vein promote the EGFR effect on Ihog stabilized cytonemes

There are four known canonical ligands for the *Drosophila* EGFR: Gurken (Grk), Vein (Vn), Spitz (Spi)³⁶ and Keren (Krn)³⁷. Three of the ligands, Spitz (Spi), Keren (Krn) and Gurken (Grk), resemble the canonical mammalian ligands and are produced as transmembrane pro-proteins, whereas Vein (Vn) resembles the non-canonical mammalian neuregulin ligands and lacks a transmembrane domain³⁸. Among them, Vn and Spi appear to be the only EGF ligands that function in the wing disc^{39,40}. We inhibited the expression of these two ligands to test their effects on cytoneme stabilization. Spi is ubiquitously expressed in wing discs. It is produced as a transmembrane precursor, which is subsequently activated by protein cleavage⁴¹ and by palmitoylation, which anchors it to the plasma membrane. These posttranscriptional modifications are carried out by the Rhomboid

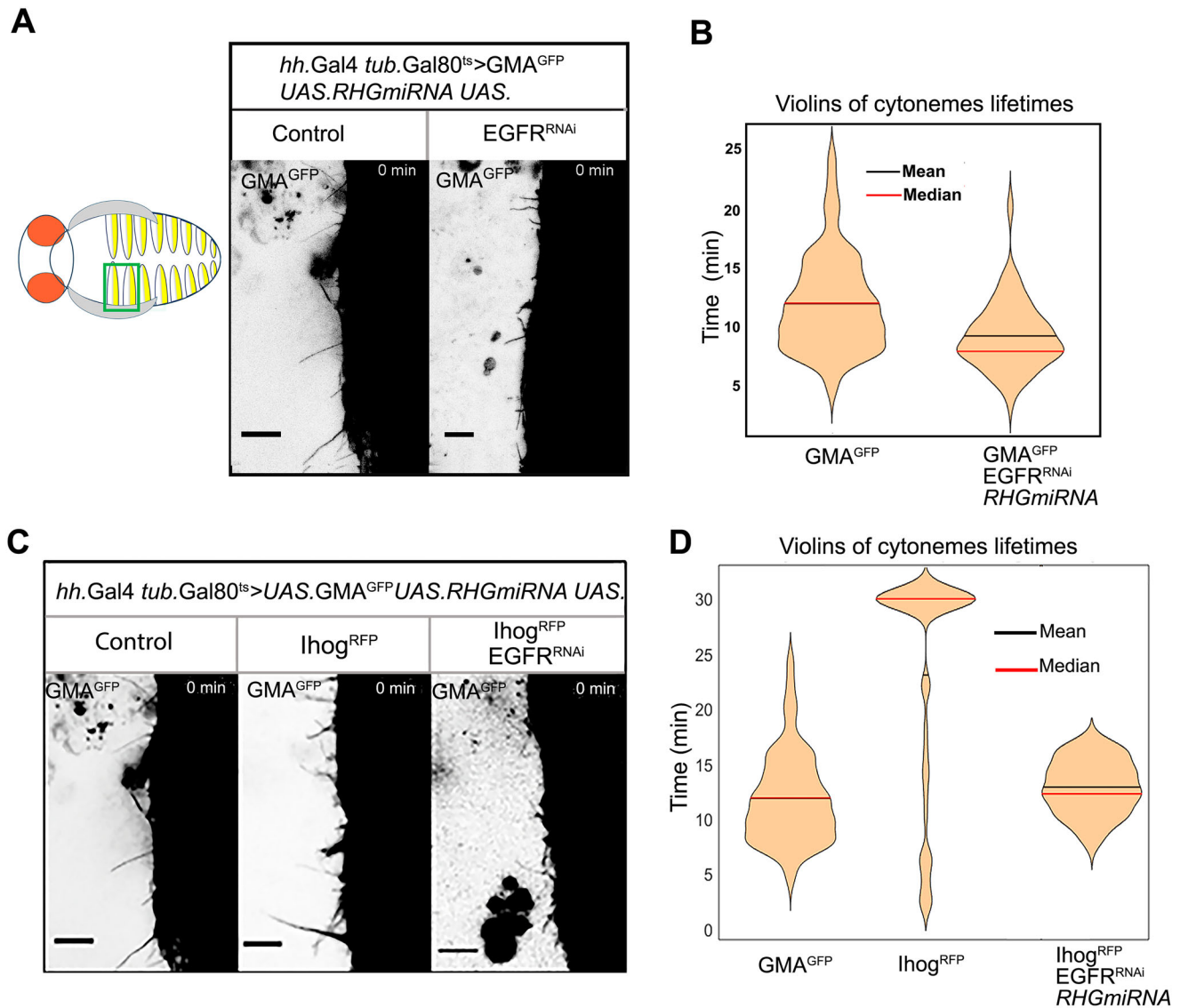


Fig. 2 | Dynamics of cytoneme in abdominal histoblasts under EGFR mutant conditions. **A** Images from movies of cytonemes protruding from abdominal histoblasts of the P compartment cells expressing UAS.GMA^{GFP} alone or expressing UAS.GMA^{GFP} and UAS.EGFR^{RNAi} at the same time for 20 h in UAS.RHGmiRNA; *hh.Gal4 tub.Gal80^{ts}* flies (see Supplementary Movie 1). Scale bars = 10 μ m. **B** Violin plots for lifetimes of cytoneme protruding from abdominal histoblasts in the same mutant conditions as in (C). Note that cytonemes after UAS.EGFR^{RNAi} expression has shorter lifetimes, indicating that they are more dynamic. **C** Images from Supplementary

Movie 2 of cytonemes protruding from abdominal histoblasts under *hh.Gal4* expressing either GMA^{GFP} alone, or coexpressing UAS.Ihog^{RFP} or UAS.Ihog^{RFP} and UAS.EGFR^{RNAi} plus UAS.RHGmiRNA at the same time to inhibit apoptosis, (see Supplementary Movie 2). Scale bars = 10 μ m. **D** Violin plots showing cytoneme lifetime in the abdominal histoblasts visualized in (C). Note that Ihog^{RFP} fails to stabilize cytonemes under EGFR downregulation conditions. Source data are provided as a Source Data file.

(Rho) protease⁴² and Rasp palmitoyl acyltransferase and their expression patterns create a spatial pattern of EGFR activity. Cleaved but non-palmitoylated Spi is released as a soluble ligand and induces a low long-range EGFR response; in contrast, palmitoylation restricts diffusion and enhances activity at a shorter range (Miura et al.³⁹). We found that Spi down-regulation by RNAi expression in the P compartment of the wing disc abrogated Ihog stabilized cytonemes along the A/P compartment border (Fig. 4B compared with A, and quantifications for normalized number D and length E). We also observed that Vn down-regulation by RNAi expression in the P compartment of the wing disc (Fig. 4C) decreased Ihog stabilized cytonemes along the A/P compartment border (Fig. 4C compared with A, and quantifications for normalized number in D, and length in E). Since Vn is induced by the Hh pathway at the A/P compartment border⁴³ we silenced Vn (Supplementary Fig. 3) in this area using *ptc.Gal4* as driver. In these

conditions, the absence of Vn affected clearly the number and length of cytonemes (Supplementary Fig. 4E compared with D, and quantification in H, I). Accordingly, the overexpression of Vn in the same area increased the number and length of Ihog stabilized cytonemes (Supplementary Fig. 4I compared with D, and quantification in H, I). The efficacy of the tools used in these studies for both gain and loss of function of Vn is shown in Supplementary Fig. 4B and C.

Since Vn and Spi are secreted proteins, we analysed if their silencing could have a non-autonomous effect. Indeed, we observed that Spi and Vn inhibition affected Hh cytonemes in a non-cell-autonomous manner, as expression of Spi^{RNAi} and Vn^{RNAi} in Hh receiving A compartment cells also reduced the number of Ihog stabilized cytonemes emanating from P compartment (Fig. 4G compared with F, and panels I, J for quantification; Fig. 4H compared with F, and panel I, J for quantification). One possible explanation to this non-autonomous effect is

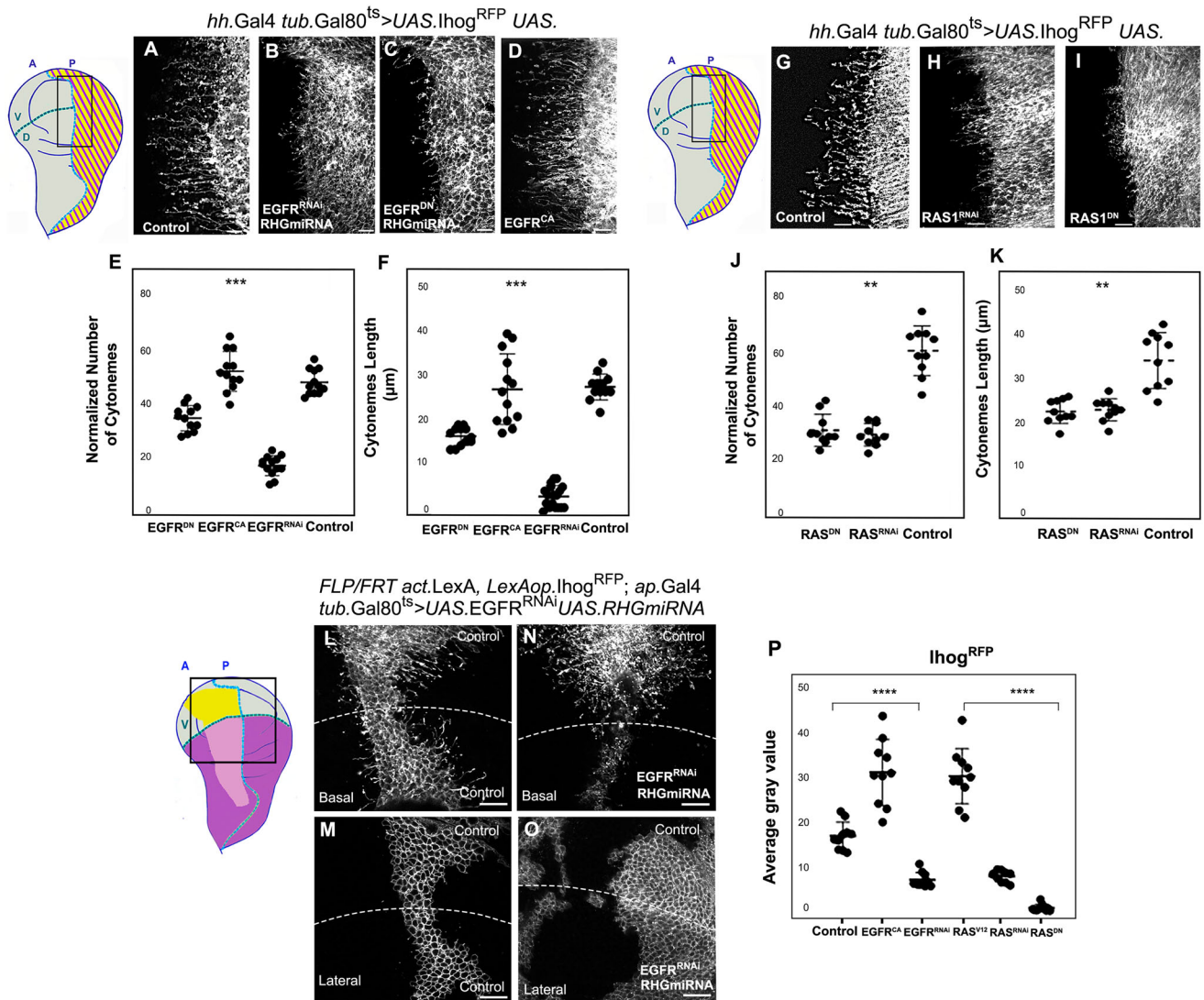


Fig. 3 | The EGFR/Ras1 pathway influences Ihog stabilized cytonemes.

A Cytonemes stabilized by Ihog^{RFP} in Hh-producing cells in *hh.Gal4 tub.Gal80^{ts} > UAS.Ihog^{RFP} UAS*. **B–D** Ihog^{RFP} stabilized cytonemes are reduced or nearly absent after transient inhibition of the EGFR by UAS.*EGFR^{RNAi}* (**B**) or UAS.*EGFR^{DN}* (**C**) and augmented by expressing a constitutively active form of EGFR (UAS.*EGFR^{CA}*) (**D**). **E** Quantification of cytonemes number within a selected window measuring the proportional 20% of the wing disc pouch size to normalize (wing discs represented by a dot). The statistical analysis performed using two-side pairwise comparisons with Wilcoxon rank-sum test shows a significant reduction after *EGFR^{RNAi}* ($p < 0.0002$), or UAS.*EGFR^{DN}* expression ($p < 0.0005$) while it marginally increased upon over-expression of UAS.*EGFR^{CA}* ($p < 0.0005$). **F** Quantification of the maximum lengths reached by cytonemes (measured as described above) reveals a significant difference between expressing UAS.Ihog^{RFP} alone and coexpressing *EGFR^{RNAi}* ($p < 0.0001$) or UAS.*EGFR^{DN}* ($p < 0.0005$), while it slightly increases with high variability upon co-expression of *EGFR^{CA}* ($p < 0.0002$). **G** Cytonemes of *hh.Gal4, tub.Gal80^{ts} > UAS.Ihog^{RFP}* wing disc

as control. **H, I** Ihog^{RFP} stabilized cytonemes are reduced after transient inhibition (for 22 h) of the Ras1 (UAS.*Ras1^{RNAi}*) (**H**) or after transient expression (for 20 h) of a dominant negative form of Ras1 (UAS.*Ras1^{DN}*) (**I**). **J, K** Quantification of cytoneme number (control, *Ras1^{RNAi}*, *Ras1^{DN}* $p < 0.002$) (**J**) and of the maximum lengths that cytonemes as in (**F**) (*Ras1^{RNAi}*, *Ras1^{DN}* $p < 0.002$) (**K**). **L–O** Wing disc containing Ihog^{RFP} expressing clones (**L, M**) and coexpressing *EGFR^{RNAi}* in the dorsal compartment (**N, O**) showing in basal sections stabilized cytonemes emanating from a clone expressing Ihog^{RFP} under normal conditions (**L**) or co-expressing *EGFR^{RNAi}* in the dorsal side, keeping the ventral side as control (**N**). Drawing model shows clones in yellow and the *EGFR^{RNAi}* expression domain in purple. Note that cytonemes protruding from cells within the EGFR downregulated area are very short or absent and that Ihog^{RFP} levels membranes severely decrease after EGFR inhibition (**N, O**). **P** Statistic analysis for Ihog^{RFP} levels expressed alone or co-expressed with *EGFR^{CA}*, *EGFR^{RNAi}*, *Ras1^{V12}*, *Ras1^{RNAi}* or *Ras1^{DN}* in the P compartment ($p < 0.0001$). The panels display the data point distribution with mean and SD whiskers. Scale bars = 10 μm. Source data are provided as a Source Data file.

that cytonemes from the A compartment cells have been compromised, somehow affecting the stability of the P compartment cytonemes.

EGF signalling maintains endogenous Ihog levels at plasma membranes

Since EGFR signalling has an impact on ectopic Ihog levels, we decided to explore this phenomenon further. It has been described that both Ihog and its homologous protein Brother of Ihog (Boi) act as Hh co-receptors⁴⁴ although with different involvements in Hh gradient

formation²¹. We have previously shown that, in contrast to Ihog, increasing the levels of Boi does not stabilise cytonemes²¹. In the current study we observed that EGFR signalling does not have the same effect on Boi levels as it does on Ihog levels (Supplementary Fig. 4). Specifically, inhibition of EGFR signalling led to a reduction in the fluorescence of ectopically expressed Ihog^{RFP} at the plasma membrane (Supplementary Fig. 4A, B, quantification in C), while ectopically expressed Boi^{YFP} exhibited a slight increase in fluorescence (Supplementary Fig. 4 D, E, quantification in F). These results are consistent

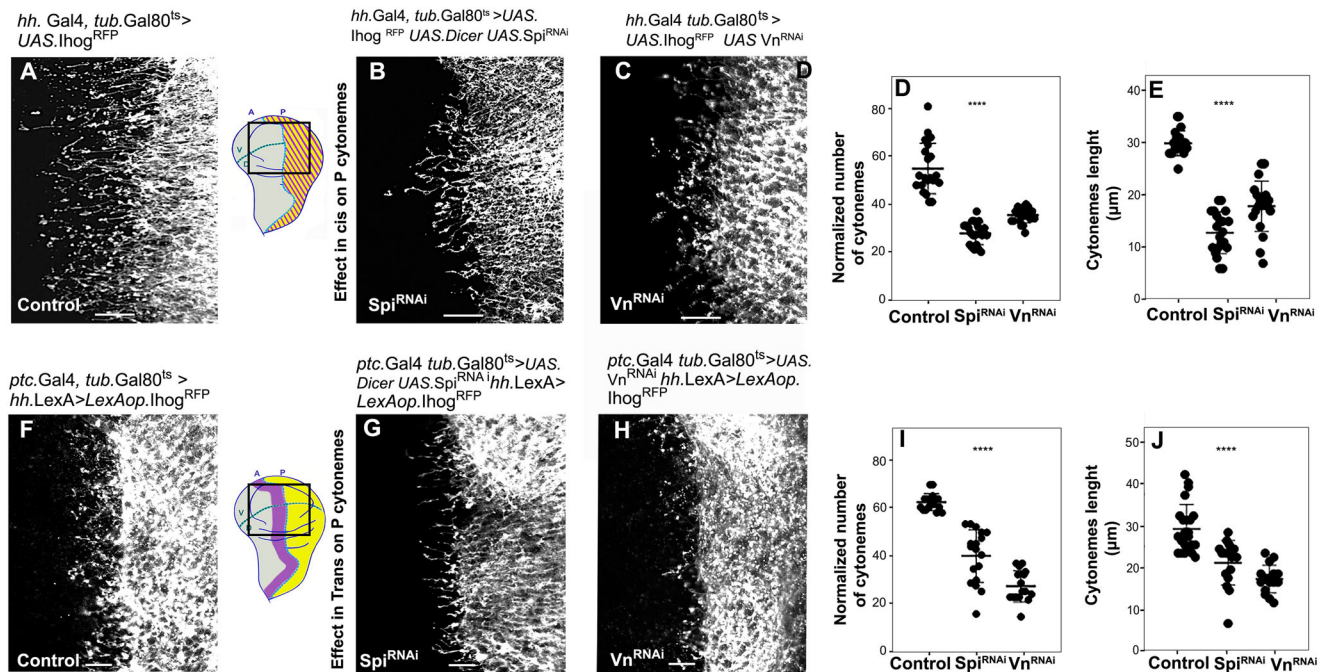


Fig. 4 | The EGFR ligands Spitz and Vein influence Ihog stabilised cytonemes. **A** Basal sections of wing discs showing Ihog^{RFP} stabilized cytonemes protruding from Hh-producing cells (P compartment) after 24 h of induction using *Hh.Gal4, tub.Gal80^{ts}* driver, as control. **B** Ihog^{RFP} stabilized cytonemes from Hh-producing cells are reduced after transient inhibition (24 h) of Spitz (UAS.Dicer UAS.Spitz^{RNAi}) in the same cells and Vein (UAS.Vein^{RNAi}) (**C**) in the same cells. Normalized number (**D**) and length (**E**) of Ihog^{RFP} stabilized cytonemes from Hh producing cells (P compartment) after transient inhibition of Spitz and Vein in the same cells (A compartment). Statistical significance two-sided with Wilcoxon signed rank test was determined with the *p*-value < 0.0001. The drawing model of a disc showing the expression of Ihog^{RFP} (yellow) and Ihog plus Spitz^{RNAi} or Vein^{RNAi} (yellow and purple lines) in the P compartment. **F** Ihog^{RFP} stabilized cytonemes in Hh-producing cells (P compartment) under LexO/LexA system (*hh.LexA>LexO.Ihog^{RFP}* wing discs) during whole development, as a control. **G, H** Ihog^{RFP} stabilized cytonemes combining

the Lex/Gal4 systems of transgene induction in *ptc.Gal4, tub.Gal80^{ts}* > UAS.Dicer UAS.Spitz^{RNAi} *hh.LexA>LexO.Ihog^{RFP}* (**G**) in a *ptc.Gal4, tub.Gal80^{ts}* < UAS.Vein^{RNAi} *hh.LexA>LexO.Ihog^{RFP}* wing discs (**H**). **I, J** The normalized number and length of Ihog^{RFP} stabilized cytonemes protruding from the P compartment in wing discs following transient inhibition (24 h) of Spitz and Vein in the receiving cell (A compartment) were analysed using two-sided pairwise comparison with Wilcoxon signed rank test (**I**: *p* < 0.0010 **J**: *p* 0.0001). Note the non-cell-autonomous effect on the stabilization of P compartment cytonemes by transient inhibition of Spitz or Vein in the A compartment cells. The drawing model of a disc shows the expression domains of UAS.Ihog^{RFP} (yellow) at the P compartment and of UAS.Dicer UAS.Spitz^{RNAi} or UAS.Vein^{RNAi} (purple) at the A compartment. Statistical analysis was performed using two-sided with Wilcoxon signed rank test for pairwise comparisons. The panels display the data point distribution with mean and SD whiskers Scale bars = 10 μ m. Source data are provided as a Source Data file.

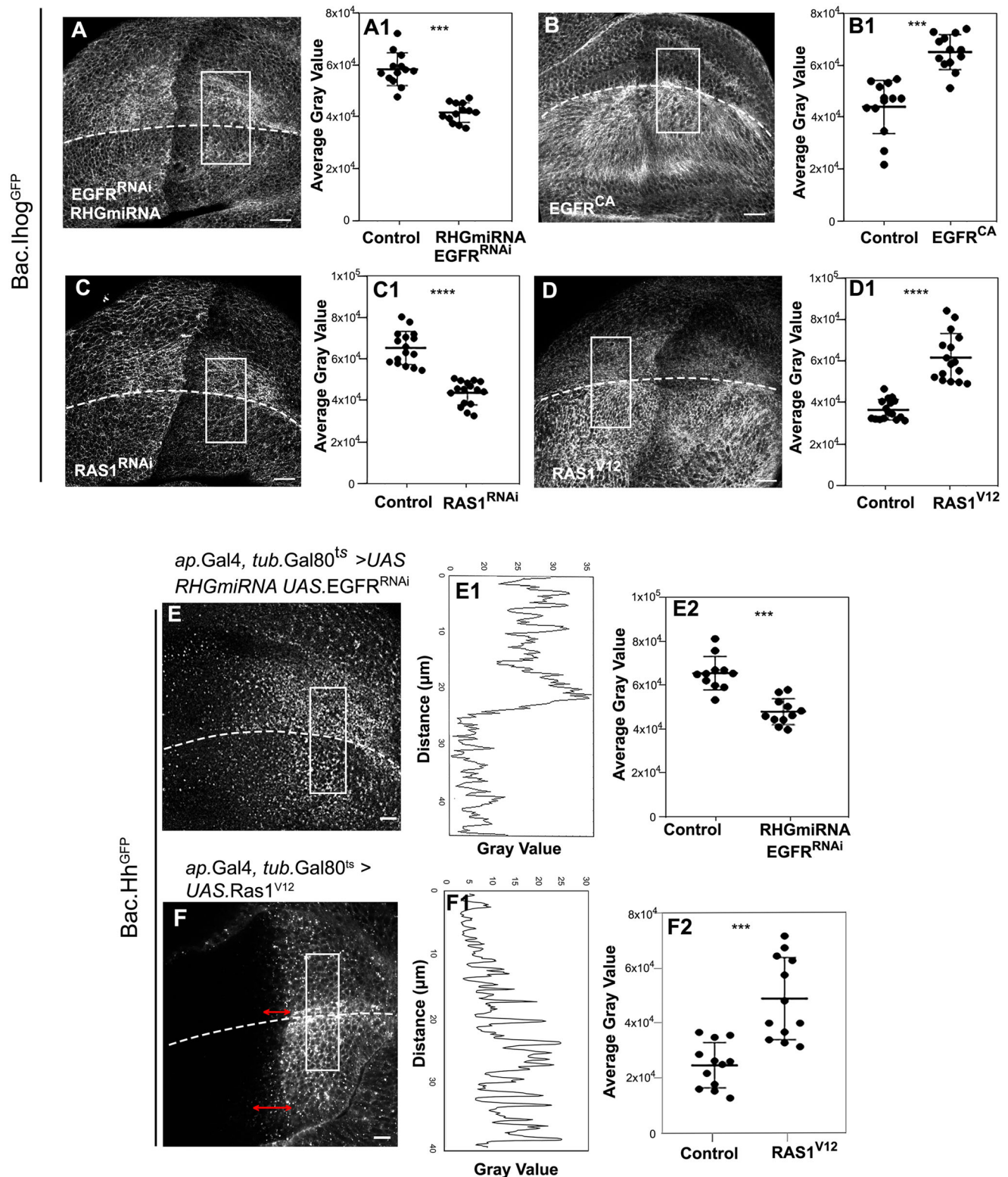
with the idea that the EGFR-dependent effect on Ihog levels in the wing disc is specific.

We next investigated whether this effect on Ihog levels occurred not only after Ihog overexpression but also at endogenous Ihog levels. We used the *Bac.Ihog^{GFP}* line, which reproduces the wild-type Ihog expression levels and expression pattern⁴⁵. After expression of EGFR^{RNAi} in the dorsal compartment of the wing disc, the levels of Ihog^{GFP} were decreased mainly in the basal region, compared to the ventral compartment (Fig. 5A, and A1 for quantifications). Conversely, Ihog^{GFP} accumulated in the basal region upon EGFR^{CA} expression (Fig. 5B and B1 for quantifications). Concerning Ras1, we found that the expression of either Ras1^{RNAi} or Ras1^{V12} had a clear effect on the basal levels of Ihog, decreasing or increasing them respectively (Fig. 5C, D, and C1, D1 for quantifications).

Concomitantly with the reduction in Ihog levels, endogenous Hh levels decreased after inhibiting EGFR activity (Supplementary Fig. 5A, B and C for quantification). This reduction is more acute basally, as shown after EGFR inhibition at the dorsal half of the wing disc compared to the wildtype ventral half (Fig. 5E and E1-E2 for quantifications). Accordingly, using the same driver, the ectopic expression of Ras1^{V12} increased the levels of Hh dorsally and the extension of the Hh gradient slightly increased (Fig. 5F, double arrows, and F1-F2 for quantifications). This effect on Hh levels is very likely a consequence of the described alteration of basal levels of Ihog^{46,47}.

Ihog expression is induced by the UAS/Gal4 system, and EGFR regulation of Ihog plasma membrane levels most likely occurs through regulation of the number of intracellular vesicles either arriving or leaving the plasma membrane, as Ihog levels at membranes decrease, but the number of fluorescent puncta increases after EGFR inhibition (Fig. 6B, G for quantification). Thus, we next explored whether the effect of EGFR loss of function on Ihog levels could be caused by affecting the intracellular pathway that moves Ihog to the membrane, or during endocytosis of Ihog and its further degradation. Under EGFR inhibition, the Ihog fluorescent punctae did not increase after transient expression of Shibire (Shi) RNAi (Shi is the *Drosophila* Dynamin-like protein) (Fig. 6D and C for comparison; quantification in G) or after blocking endocytosis by treatment with Dynasore (Fig. 6E–F1). These findings suggest that the absence of EGFR signalling reduces Ihog levels at the membrane by enhancing its endocytosis and degradation. To address this, we in vivo incubated discs overexpressing Ihog^{GFP}, with or without co-expressing EGFR^{RNAi}, in the presence of fluorescent Dextran-647 to analyse internalized vesicles, and of LysoTracker-RFP to analyse lysosomes. The number of Dex-647 and LysoTracker-RFP punctae increased in cells which co-expressed Ihog^{GFP} and EGFR^{RNAi} (Fig. 6H, I and insets to split channels). These results indicate that the absence of EGFR pathway increases endocytosis and lysosomal degradation of Ihog.

ap.Gal4, tub.Gal80^{ts} >UAS.



Ihog interacts with cytoskeleton and plasma membrane regulators

Previous data have shown that Ihog extracellular FN domains are essential for ligand reception, Ihog dimerization and Ihog interactions with the glypicans Dally and Dally-like protein (Dlp)^{21,24,48}. The interactions of Ihog and the glypicans are important for cytoneme

dynamics²¹ and for their orientation perpendicular to the A/P compartment border as proposed by mathematical modelling²³. No interactions of Ihog have been described other than with glypicans, Hh and its receptor Ptc; we thus set up to identify Ihog interacting proteins. To that end, we undertook proteomics to isolate potential Ihog-interacting proteins. Extracts of whole 3rd instar larvae expressing

Fig. 5 | EGFR/Ras1 pathway regulates the endogenous levels of Ihog and Hh. **A–D1** Basal section of a wing disc expressing Ihog^{GFP} at endogenous levels (*Bac.ihog^{GFP}*) while either EGFR or Ras1 are silenced in the dorsal half in *ap.Gal4 tub.Gal80^{ts} > UAS.RHGmiRNA* discs. Note the decreased levels of basal Ihog^{GFP} in the dorsal half of the disc after EGF, Ras1 downregulation (24 h). **B, D** Basal section of a wing disc expressing *Bac.ihog^{GFP}* while ectopically expressing either a constitutively active form of EGFR (*UAS.EGFR^{CA}*) or *UAS.Ras1^{V12}* in the dorsal half for 18–20 h. Note the increased levels of basal *Bac.ihog^{GFP}*. **A1–D1** Quantifications of Ihog^{GFP} at endogenous levels are presented as mean gray values within a selected window for normalization. Statistical analysis (**A1** and **B1** $p < 0.0002$, **C1** and **D1**: $p < 0.0001$) showed significant differences between control and inhibiting treatments for EGFR and Ras1 while enhancing activity of EGFR and Ras1^{V12} showed an increase. **E–E2** Basal section of an *ap.Gal4, tub.Gal80^{ts} Bac.hh^{GFP} > UAS.RHGmiRNA, UAS.EGFR^{RNAi}* wing disc that expresses EGFR^{RNAi} only at the dorsal half of the wing disc, keeping

the ventral side as an internal control. **E1** Graphical representation of the signal values in a crop including the ventral and dorsal sides. **E2** Statistical analysis showed the reduction in Hh signal levels after EGFR downregulation ($p < 0.001$). **F–F2** Basal section of an *ap.Gal4, tub.Gal80^{ts} > UAS.Ras1^{V12}* wing disc stained with an α Hh antibody and expressing Ras1^{V12} only at the dorsal half of the wing disc, keeping the ventral side as an internal control. The double arrows indicate the increased extension of the Hh gradient after expression of Ras1^{V12}. **F1** Graphical representation of the signal values within a crop including the ventral and dorsal sides. **F2** The statistical analysis was performed using two-sided Wilcoxon signed rank test for pairwise comparison ($p < 0.0005$). The panels display the data point distribution with mean and SD whiskers. Note the increase in Hh signal levels and gradient extension (double arrows) are increased after Ras1^{V12} overexpression. Scale bars = 10 μ m. Source data are provided as a Source Data file.

Ihog^{RFP}, under the control of the UAS promoter driven by the ubiquitous driver (*Actin.Gal4*) were incubated with RFP-Trap-A and subjected to affinity purification-mass spectrometry. Extracts from larvae expressing RFP alone were used as a negative control. Recognising the preliminary nature of these results we focused validation on a set of candidate proteins with ontologies related to the cytoskeleton and vesicular trafficking; proteins that may be required for Hh signalling in the wing disc (Fig. 7A). After transient RNAi expression for chosen candidates in Hh-producing cells, we measured Hh signalling activity and gradient formation using the *ptc.enhancer-trap-GFP* reporter. To validate this setup, we first analysed the response of this reporter of Hh signalling gradient under EGFR^{RNAi} expression (Supplementary Fig. 6A–C for quantification). Using this *ptc.enhancer trap-GFP ptc.enhancer-trap-GFP⁴⁹* reporter, most of the expressed RNAi constructs directed against the selected candidates decreased Hh signalling gradient (Fig. Supplementary 6D).

The Ihog intracellular domain recruits and focalizes Cheerio to the plasma membrane

Based on the preliminary proteomic analysis, we further selected Cheerio (Cher), the filamin A ortholog, for further investigation. Our observations revealed that down-regulation of the actin cross-linker Cher significantly reduced both the number and length of Ihog-stabilized cytonemes (Fig. 7B–E for quantifications).

To explore further the basis of Ihog interactions with Cher, we assessed Cher levels under conditions of Ihog overexpression. By expressing Ihog^{GFP} in the P compartment, we monitored endogenous Cher levels using the Cher^{YFP} knock-in allele (*cher-YFP-Trap*)⁵⁰. Our results showed a significant recruitment of Cher at the basal side of the disc epithelium, where cytonemes labelled by both Ihog^{RFP} and Cher^{YFP} were clearly visible (Fig. 7F, F2). Quantifications of these interactions are provided in Fig. 7G.

We also analysed the interaction between Ihog and Cher following Ihog silencing. Using RNAi to knock down Ihog expression in the dorsal region of the disc, we observed a reduction in Cher^{YFP} levels compared to the basal Cher^{YFP} levels in the ventral side, which served as the control (see Fig. 7H and I for quantification). This Ihog-Cher interaction is further supported by the co-immunoprecipitation results from tissues co-expressing Cher^{YFP} and Ihog^{RFP} (Fig. 7J).

Next, we analysed Cher^{YFP} levels after expressing Ihog^{RFP} in the dorsal side of the wing disc, using an anti-GFP antibody to prevent signal overlap between RFP and YFP. While the increase in Cher^{YFP} levels was less pronounced in lateral sections compared to basal sections, Cher appeared as bright dots in the dorsal cells, suggesting the protein was concentrated in small foci (Fig. 8A, insets from panel A1, a, a'; and C for quantification). Expression of Ihog constructs lacking the C-terminal intracellular region (Ihog Δ C) did not promote Cher^{YFP} focalization at the membrane, resulting in a uniform Cher^{YFP} distribution (Fig. 8B, B1, insets b, b'; and D for quantifications). This indicates that high levels of the Ihog intracellular domain are necessary to

recruit Cher^{YFP} to membrane-associated foci. To further visualize Cher focalization, we expressed Ihog^{GFP} in the large salivary gland cells of Cher^{YFP} larvae, where increased Cher^{YFP} at the cell membranes appeared as focalized patches (Fig. 8E–F1, and G for quantifications).

Since EGFR signalling enhances Ihog levels at the basal plasma membrane, it may also play a role in recruiting Cher. Notably, silencing EGFR in the dorsal part of the wing disc led to a reduction in endogenous Cher^{YFP} levels (Fig. 8H, and I for quantification), suggesting an interaction between EGFR and Cher, consistent with previous reports of the Ras1^{V12} and Cher interaction^{51,52}.

Discussion

The EGFR pathway regulates cytoneme dynamics

EGF signalling as a protrusion promoter has been investigated, especially for cell motility during metastatic processes^{25,26,29}. EGF signalling triggers rapid actin cytoskeleton reorganisation factors, one of the earliest responses following EGFR activation^{27,28}. Here we present evidence for a role of the EGFR signalling cascade also on cytoneme regulation and Hh signalling function. In particular, down-regulation of the EGF pathway results in more dynamic cytonemes (Supplementary Movies 1 and 2), which could lead to an unstable association with Hh and aberrant Hh signalling. It is interesting to note that a reduction of the Hh gradient was observed after inhibiting the EGFR/Ras1 pathway either in Hh receiving cells (A compartment) or Hh presenting cells (P compartment), suggesting that the EGFR effect on Hh signalling might occur via the regulation of cytoneme dynamics.

EGFR/Ras1 activity is required for Ihog polarized presence at plasma membranes

Our results provide evidence that EGFR signalling reduces cytoneme stabilization, at least in part, through the regulation of Ihog levels at the basal plasma membrane. The lack of Ihog-induced stabilization of cytonemes in EGFR mutant background could also occur as consequence of its effect on reducing ectopic Ihog levels. Thus, we have found both a lack of Ihog-induced stabilization of the cytoneme and a decrease in the levels of Ihog at the plasma membrane following inhibition of EGFR/Ras1. These properties are specific to the Ihog, since EGF signalling does not have the same effect on Boi, the other Hh coreceptor, what is not unexpected since cytoneme stabilization is a property of Ihog but not of Boi²¹.

Membrane trafficking regulation of the EGF receptor is key to recruit different components of the cytoskeleton regulatory proteins at the plasma membrane³¹, as well as to reach the onset of some of their responses⁵³. Here we have described that the expression of constitutively active forms of EGFR and Ras1^{V12} increases the basolateral presence of endogenous Ihog (*Bac.ihog^{GFP}*). Conversely, the blockade of EGFR or Ras1 by RNAi leads to a reduction in Ihog levels. EGFR/Ras1 pathway also affects the levels of the endogenous Hh mainly in the basal part of the wing disc epithelium. This reduction could be a direct consequence of reduced Ihog levels since it has previously described

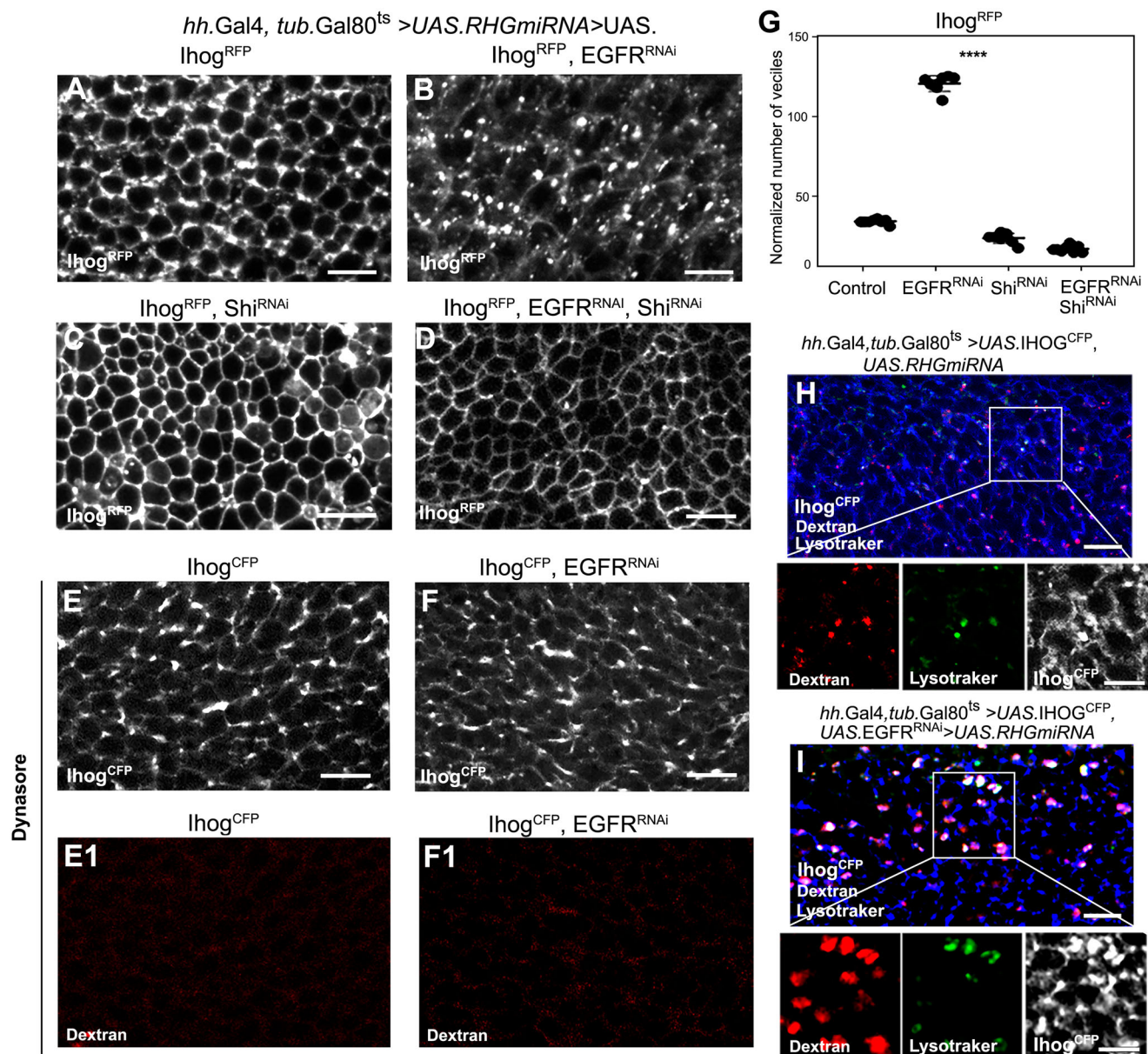


Fig. 6 | Ihog at membranes is withdrawn by endocytosis and degradation. **A–D** Crops from a lateral section of *hh.Gal4, tub.Gal80^{ts} > UAS.RHGmiRNA* wing discs expressing UAS.Ihog^{RFP} (**A**), UAS.Ihog^{CFP} and UAS.EGFR^{RNAi} (**B**), UAS.Ihog^{RFP} and UAS.Shi^{RNAi} (**C**) or UAS.Ihog^{RFP} plus EGFR^{RNAi}, together with UAS.Shi^{RNAi} to block endocytosis (**D**). Note a severe increase in puncta numbers after EGFR down-regulation. Note also that Ihog^{RFP} levels at plasma membranes decrease after inhibition of EGFR but are significantly rescued when endocytosis is simultaneously inhibited. Scale bars = 10 μ m. **E–F1** Incubation with Dynasore, inhibitor of the GTPase activity of Dynamin, at 25 °C for 40 min, prior to incubation with 3.7 mM Dextran-647 for 10 min. Note the increases Ihog^{CFP} in the plasma membrane after

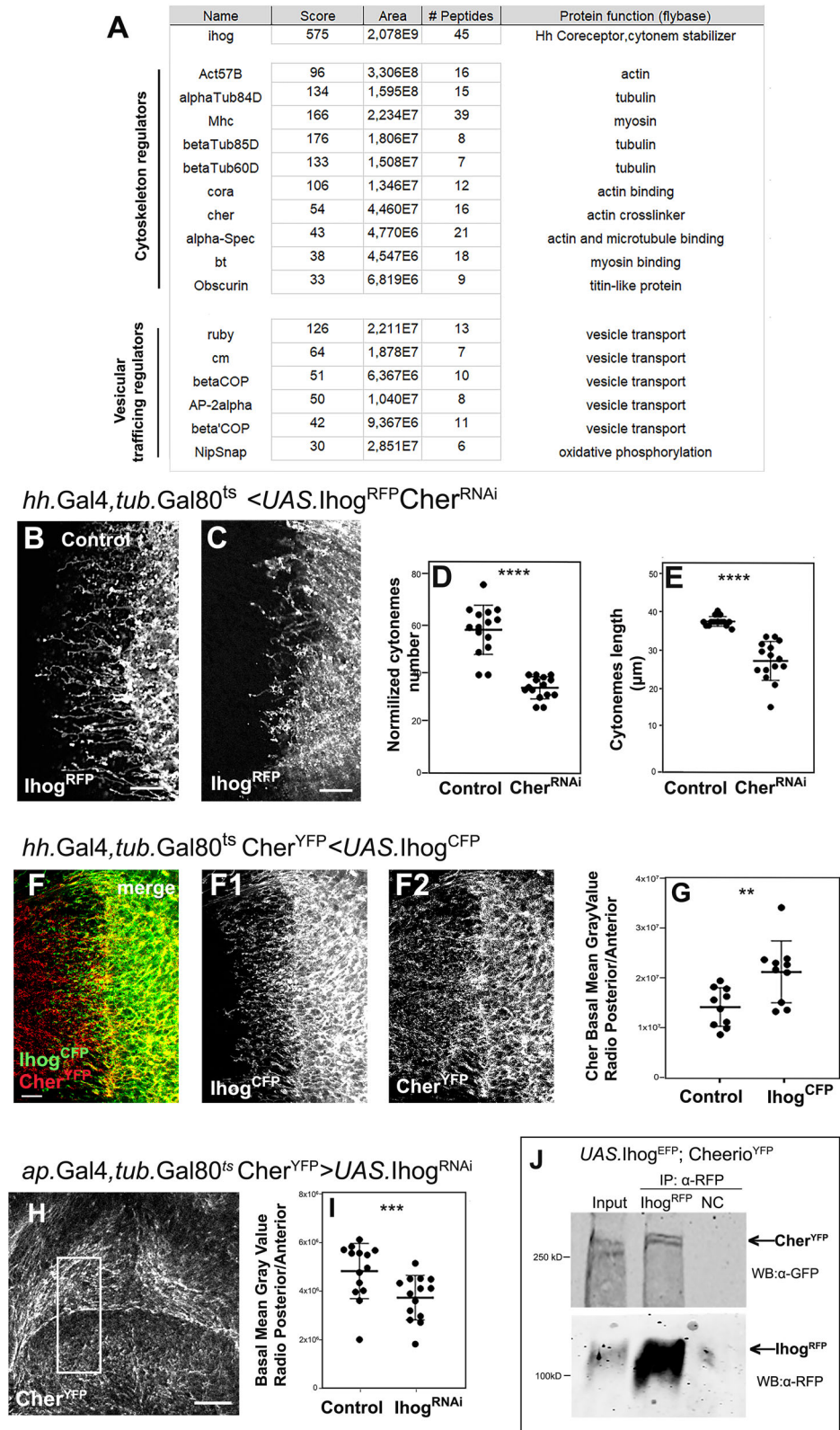
UAS.EGFR^{RNAi} expression (**E, F**). Note also the absence of Dextran labelled vesicles (**E1, F1**). **G** Vesicle-like puncta were quantified within a defined area for the three treatment conditions. A total of 8 wing discs per treatment were analysed, and a ANOVA test was performed, yielding p -value < 0.0001. **H, I** Crops of lateral sections of *hh.Gal4, tub.Gal80^{ts} > UAS.RHGmiRNA* wing discs expressing Ihog^{CFP} as control (**H**) and UAS.Ihog^{CFP} together with UAS.EGFR^{RNAi} (**I**) and incubated with 100 nM Lysotracker (green) for 40 min at 25 °C and for the last 10 min with 3.7 mM Dextran-647 (red). Scale bars = 10 μ m. The split channels in the amplified insets show in more detail the increase of Dextran and Lysotracker vesicles after EGFR^{RNAi} expression. Scale bar = 5 μ m. Source data are provided as a Source Data file.

that Ihog is required to maintain normal Hh extracellular levels^{46,47}. The normal prevalence of Ihog at basal plasma membranes has been previously described^{44,47}, and it correlates with the localization of cytonemes at this basal level of the wing disc epithelium^{6,47,54}. Furthermore, the EGF-dependent reduction on ectopic Ihog levels at the plasma membrane is almost completely annulled if endocytosis is blocked, suggesting that an EGF-reliant membrane recycling regulatory mechanism ensures localization of Ihog to the basal plasma membranes.

The capacity of Ihog to stabilize cytonemes has been related to Ihog interactions with itself and with the glypicans Dally and Dally-like

at cytoneme contacts^{21,23}. These interactions carried out through the extracellular FN domains of Ihog, are involved in cytoneme stabilization^{21,24} and might be responsible for cytoneme orientation perpendicular to the A/P compartment border²³. Moreover, recent research has found that Ihog interacts through its extracellular domains with integrins, contributing to regulate integrin distribution and thus integrin-mediated basal focal adhesion⁵⁵.

While these interactions primarily occur extracellularly, we have shown that the Ihog intracellular domain co-operates with actin cytoskeleton regulators, such as the actin cross-linker Cher (Fig. 8). This interaction is influenced by EGFR activity through recruitment of



Cher towards plasma membranes, focalizing this actin cytoskeleton modulator to membrane domains. Thus, we show here that the EGFR pathway may serve a dual purpose in cytoneme stabilization: one involving the regulation of Ihog levels on the plasma membrane, and the other pertaining the modulation of intracellular cytoskeletal dynamics. In summary, we have uncovered a possible mechanism for regulating Hh cytoneme dynamics, which influences the levels of the Hh co-receptor Ihog.

Pathway cooperation in cytoneme-mediated signalling

Cytonemes and related structures, such as tunnelling nanotubes, are used by cancer cells to communicate with each other and with stromal cells^{56–61}. The wing imaginal disc has been used extensively to study the progression of tumours [reviewed by ref. 34]. The induction of groups of cells over-expressing an oncogenic-activated form of Ras1 in the wing disc results in hyperplastic growth as a consequence of increased cell growth, accelerated G1-S transition and cell shape changes⁶². We

Fig. 7 | Ihog proteome reveals its interaction with membrane and cytoskeleton regulators. **A** A list of proteins specifically isolated from Ihog^{RFP} affinity purification, with known protein functions relating to cytoskeleton and vesicular trafficking. **B–E** Cytonemes stabilized by Ihog^{RFP} expression decrease after transiently inhibiting the actin regulator Cher ((C) compared with the control (B)). **D** Boxplots showing the quantification of the maximum distance reached by cytonemes within a window measuring the proportional 20% of the wing pouch size to normalize. The statistical analysis performed using two sided pairwise comparison with Wilcoxon tests showed a significant effect of treatment as length decreased after Cher^{RNAi} expressions ($p < 0.0001$). **E** Cytoneme number shows a more moderate reduction after inhibition of Cher ($p < 0.0001$). **F, G** Basal sections of Cher^{YFP} (red) wing discs expressing at endogenous levels and expressing UAS.Ihog^{CFP} (green) in the P compartment. Note the stabilization of cytonemes induced by Ihog^{CFP} and the colocalization of Ihog and Cher^{YFP} in cytonemes (**F1, F2**). **G** Quantifications of basal

mean gray values of the dorso/ventral ratio of Cher^{YFP} were analysed using two sided pairwise comparison with Wilcoxon tests ($p < 0.002$). The panels display the data point distribution with mean and SD whiskers. Note also the increased levels of Cher^{YFP} in the P compartment, probably due to the recruitment by ectopic Ihog (G2). **H** Basal section of a Cher^{YFP} wing disc expressing UAS.Ihog^{RNAi} in the dorsal compartment. Note the downregulation of Cher^{YFP} in the absence of Ihog. **I** Quantifications analysed by two-sided pairwise comparison with Wilcoxon test showing the decrease of the Cher^{YFP} after Ihog^{RNAi} expression in the dorsal compartment ($p < 0.0002$). **J** Co-immunoprecipitation experiment of larvae extracts expressing UAS.Ihog^{RFP} and endogenous Cher^{YFP}, using α -RFP antibody for immunoprecipitation and α -GFP antibody for western blot development, while no protein is observed in the extracts expressing RFP alone as negative control (NC). Scale bars = 10 μ m. Source data are provided as a Source Data file.

have shown that these changes are also associated with changes in cytoneme dynamics as EGFR signalling has been found connected with an increase in cytoneme-mediated transport of Wg, Dpp and Df from epithelial to mesenchymal cells, leading to an increase in the mesenchymal cell population⁵⁹.

Signalling integration between two major signalling pathways, EGF and Hh, mediated by transcriptional regulation has been shown to happen during development in *Drosophila*^{43,63} or during tumorigenic processes in mammals^{64,65}. A further type of cooperation is conceivable with the existence of a multi-component signalling complex involving EGFR, Vn, Ihog, Boi and Hh based on a direct interaction between Vn, and Ihog through their respective Ig domains⁶⁶.

The pathway cooperation we have described might involve rapid membrane trafficking responses to regulate Ihog levels as well as actin cytoskeleton remodelling following EGF signalling activation. These changes influence cytoneme dynamics and Hh signalling. Signalling pathway cooperation contributes and probably guarantees several different outcomes from a few signalling molecules. Thus, understanding the mechanisms of signalling cooperation is pivotal to comprehend normal development as well as its potential oncogenic consequences.

Methods

Fly mutants

A description of mutations, insertions and transgenes is available at Fly Base (<http://flybase.org/>): most of the stocks were available in Bloomington *Drosophila* Stock Centre (BDSC), Indiana, USA; <https://bdsc.indiana.edu/>; *aos-LacZ* (BDSC #2513), *tub.Gal80^{ts}* (BDSC #7019), *act FRT LexA cassette*⁶⁷, *LexAop.tub.Gal80* (BDSC # 32217) and *ap.LexA* (BDSC #54268), *cheerio.YFP-Trap* (*cher*^{CPT1001399} and *cher*^{CPT1000847})⁵⁰ (Kyoto DGGR, <https://kyotofly.kit.jp/cgi-bin/stocks/index.cgi>), *Bac.hh^{SjGFP}* and *Bac.boi^{GFP}* and *Bac.ihog^{GFP45}*, *ptc-promoter-trap-GFP* (P{PTT-GB}*ptc*^{CB02030}) (<http://flytrap.med.yale.edu>)⁴⁹.

Overexpression experiments

The Gal4 drivers: *ap.Gal4*⁶⁸, *hh.Gal4*⁶⁹, *ptc.Gal4*⁷⁰, *tub.Gal4* (BDSC #5138), *act5c.Gal4* (BDSC #255374), *ab1.Gal4* (BDSC #1824) was used to generate ectopic expression of the UAS line. The UAS-transgenes were: UAS.Ihog^{CFP}, UAS.Ihog^{RFP6}, UAS.Ihog Δ ^{RFP21}, UAS.GMA^{GFP} (BDSC #31775)⁷¹, UAS.EGFR^{CA} (BDSC #9533), UAS.EGFR^{DN} (BDSC #5364), UAS.Ras1^{DN} (BDSC #4845), UAS.Ras1^{V12} (BDSC #4847) (Felix and Rubin⁷²) and UAS.Vein (Chromosome III, a gift from A. Simcox; Schnepf et al.³⁸).

The *LexA* driver *hh.LexA*⁸ used to direct expression of *LexO.Ihog^{RFP21}*.

All RNAi lines were obtained from the BDSC and from the VDRC. The UAS.RNAi lines targeting EGFR (VDRC #v10713(II), #v103523 (II), BDSC#36770 (III) and BDSC#36773(III)), *spitz* (VDRC#102402, {KK103817}), *vein* (VDRC#v109437(II), {KK108432}), *Ras1* (VDRC#v28129GD{12553} (II)), *shibire* (BDSC #28513 and

#36921), *cheerio* (BDSC #35755), *coracle* (BDSC #35003), *nipSNAP* (BDSC#34887), *ruby* (BDSC#32477), *ihog* (VDRC#v102602,{KK112149}), *boi* (VDRC#v108265,{KK103113}) were used. An expression period between 14 and 24 h, depending on knock-down efficacy or the expression levels of the UAS-constructs, was achieved using each Gal4 combined with *tub.Gal80^{ts}* (BDSC #7019), maintaining the fly crosses at 18 °C and transferring them to the restrictive temperature (29 °C) before dissection to inactivate the Gal80. To avoid possible effect in cell death by knocking-down the EGFR (using the UAS.EGFR^{RNAi} or UAS.DER^{DN}) we coexpressed the apoptosis inhibitor UAS.RHGmiRNA, that contains *rpr*, *hid*, and *grim* sequences⁷³. The UAS-Ihog was not induced for time longer than 24 h because Ihog is an adhesion molecule that can affect cell structure. To increase the penetrance of the *spitz* RNAis, it was coexpressed with the UAS.Dicer (BDSC #24650).

For those cases in which we wanted to limit the expression of the Ihog transgene to small cell populations, clones were achieved using the FLP/FRT system. The random mosaic recombinant clones were induced with an active *act.LexA* driver⁶⁷ that induces *LexO.Ihog^{RFP8}* through a heat shock (HS) at 37 °C for 15 min at a specific developmental stage.

Efficacy of EGFR or Ras1 tools in the wing disc epithelium

To inhibit or activate the EGFR/Ras1 pathway, RNAi directed against the EGFR or Ras1 genes, as well as a dominant negative form or an activated form of these two genes, were independently expressed in wing discs. To confirm the efficacy of our tools we monitored the expression of the EGFR pathway reporters phospho-ERK⁷⁴ and Argos-LacZ (Aos-LacZ)⁷⁵. We expressed the EGFR pathway tools in the dorsal compartment cells of the disc (*ap.Gal4* driver) and used the ventral side as control. The expression levels of these reporters were reduced after transient expression of EGFR^{RNAi}, Ras1^{RNAi} or a dominant negative form of EGFR and Ras1; they were activated by constitutive active form of EGFR (EGFR^{CA}) and by the oncogenic form of Ras1 (Ras1^{V12}) (Supplementary Fig. 1).

Immunostaining of imaginal discs

Immunostaining was performed according to standard protocols⁵⁴. Imaginal discs from 3rd instar larvae were fixed in 4% (w/v) paraformaldehyde (PFA)/PBS for 20 min at room temperature (RT) and permeabilized in 10% Triton X-100 (Sigma)/PBS before incubating with 1% BSA for blocking (1 h at room temperature) and primary antibody incubations (overnight at 4 °C). For in vivo analysis of the cytoneme number and length labelled with UAS.GMA^{GFP}, the imaginal discs were fixed with 2% paraformaldehyde (PFA)/PBS for 10 min at room temperature before mounting in mounting media (Vectashield). Incubation with fluorescent secondary antibodies (1:200 Jackson laboratories and Invitrogen) was performed for 2 h at room temperature for posterior washing and mounting in mounting media (Vectashield). Antibodies were used at the following dilutions: mouse monoclonal α -Ptc, 1:150⁷⁶; rabbit polyclonal α -GFP, 1:100 (Roche); rabbit polyclonal

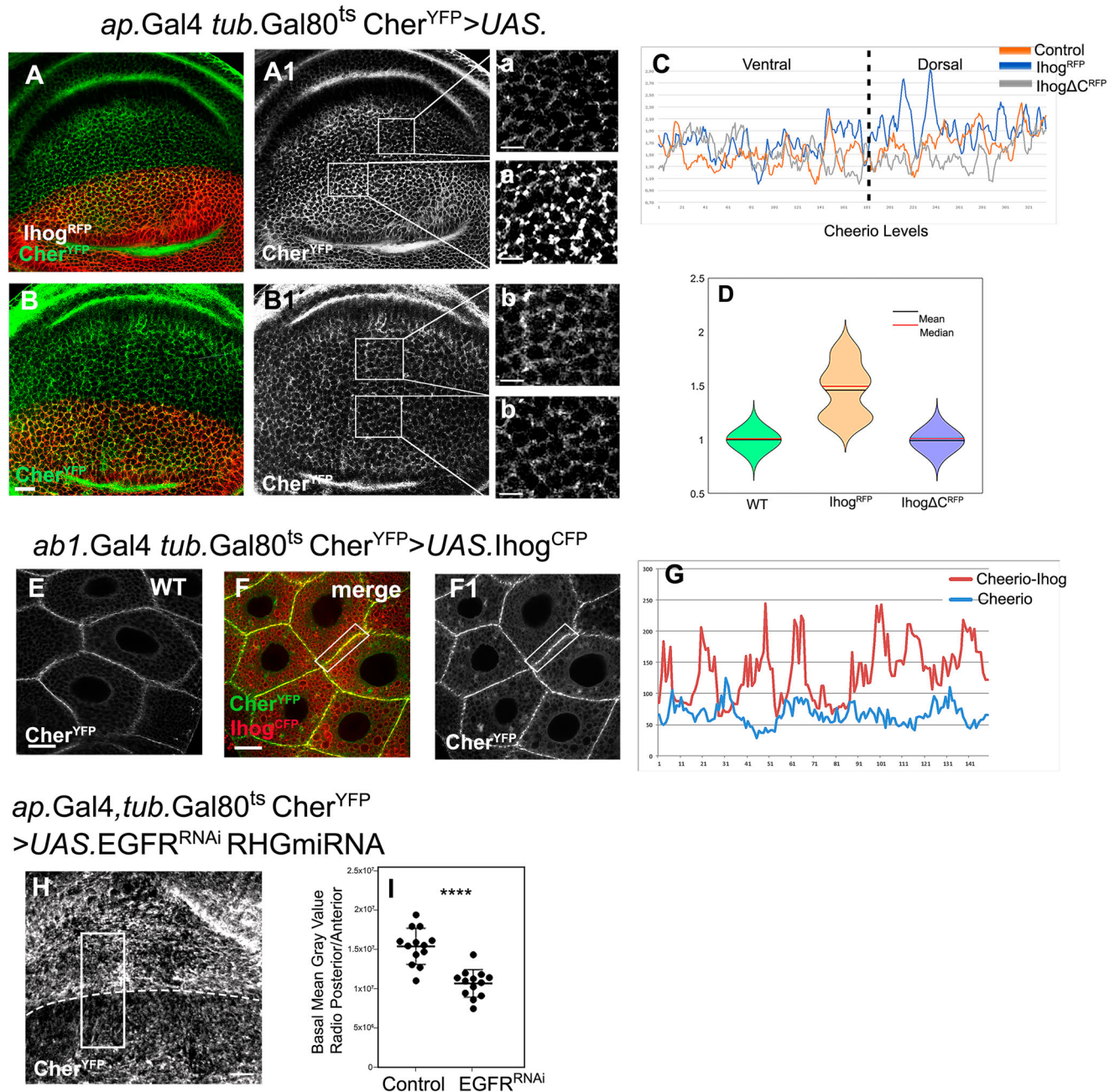


Fig. 8 | Ihog expression focalizes Cheerio at the plasma membrane. A–a' Cher^{YFP} (green) wing disc expressing Ihog^{RFP} (red) at the dorsal compartment, keeping the ventral half as control. To analyse the co-localization of Ihog^{RFP} and Cher^{YFP}, the samples were immunostained with an α -GFP antibody. **A1** Cher^{YFP} in grey. **a, a'** Enlarged insets showing Cher^{YFP} expression. Note the increased focalization of the Cher signal to spots at the plasma membrane upon overexpression of Ihog^{RFP} (**a'**). **B–b'** Cher^{YFP} (green) wing disc expressing UAS.Ihog ΔC^{RFP} (red) at the dorsal half, keeping the ventral half as control. **B1** Cher^{YFP} in grey. Note the focalization effect over Cher is lost when Ihog lacks the C-terminal region (**b, b'**). **C** Representation of the Cher^{YFP} signal in **A** and **B** within an area in normal conditions (orange), after UAS.Ihog^{RFP} (blue) or after UAS.Ihog ΔC^{RFP} expression (grey). Note the Cher^{YFP} signal after Ihog^{RFP} expression presents picks of punctual signal more intense than after Ihog ΔC^{RFP} expression. **D** Quantification of the Cher signal distribution as a ratio between the signal standard deviation from equal areas within the dorsal and ventral halves (control) to normalize (wing discs per treatment for WT $n = 7$, for

Ihog $n = 5$, for Ihog ΔC^{RFP} $n = 7$). Statistical analysis showed the rate values for Cher signal distribution when UAS.Ihog^{RFP} (orange) is expressed ($p < 0.01$) and no difference with wild type (green) or after expressing UAS.Ihog ΔC^{RFP} (blue) ($p = 1$). **E–G** Cher^{YFP} salivary gland cells showing Cher protein relocalization by Ihog^{RFP} (red) overexpression. Cher^{YFP} channel (green, grey) shows a drastic focalization of the Cher signal to spots at the plasma membrane upon overexpression of Ihog^{RFP} (**F1** compared to **E**). **G** Graphical representation of (**F**) under normal conditions (blue) and after Ihog^{RFP} overexpression (red). Note the increase in signal levels and the higher picks indicating Cher focalization to small segments within the membrane. **H** Basal section of a Cher^{YFP} wing disc after UAS.EGFR^{RNAi} and UAS.RHGmiRNA in the dorsal side. **I** Quantifications analysed by two sided pairwise comparison with Wilcoxon test show the downregulation of Cher^{YFP} in the absence of EGFR ($p < 0.0001$). Scale bars = 10 μ m, enlarged inserts 5 μ m. Source data are provided as a Source Data file.

α -B-Gal, 1/3000 (Cappel), rat monoclonal α -Ci, 1:50 (gift from R. Holgreen), rabbit polyclonal α -Hh (1/500) (gift from T. Tabata) and rabbit polyclonal α -Phospho p44/45 MAPK (ERK) antibody, 1:500 (Cell Signaling Technology).

In vivo imaging of the abdomen

Pupae were filmed through a window in the pupal case and analysed as described previously⁶. Briefly, white prepupae were attached to double-sided adhesive tape to remove the operculum with forceps. The prepupa was removed from the adhesive using water and moved to a new slide mounting between four bands of Parafilm arranged in parallel lines to ensure minimal squashing by coverslip. To avoid dehydration, a water pool was used to surround the prepupa.

Microscopy and image processing

Confocal fluorescence imaging of imaginal discs and in vivo imaging of the white prepupae abdomen were performed using a Zeiss LSM710 and LSM800 laser scanning confocal microscope, respectively. Image processing and macro development to quantify fluorescence levels were carried out using ImageJ software (National Institutes of Health).

Statistical analysis

Figures, figure legends and source data provide details of statistical analyses and sample sizes. Statistical analysis was carried out in R⁷⁷ and MatLab⁷⁸. The Matlab script was designed to organise the data, compute statistical analysis, and present results in violin plots (see supplementary file 1). The kernel bandwidth (bw) for the violins shape was selected to better visually represent the data in each plot (bw = 0.1–2). All data sets were tested for normality using Shapiro-Wilk tests. Where appropriate, based on the normality results, ANOVA or two-sided pairwise comparisons using the Wilcoxon test were performed.

Quantification of gradient length

Gradient lengths were determined in rectangle areas and then expressed as a proportion of the wing pouch size measuring the response of the Hh target Ptc y Ci through antibody staining by ImageJ plot profile comparing signal from dorsal and ventral sides of wing discs. Values from a fixed area (580 × 175 px) in each half of the disc. The statistical analysis of 10–15 discs was done with GraphPad 9.

For gradient lengths using the *ptc.enhancer.trap-GFP*⁹, GFP signal was measured over the confocal images with plot profile tool of FIJI (with a same ROI size), and later processed in a Matlab script where we removed the background fluorescence signal and each sample was normalized to its maximum; lengths were normalized to the wing pouch size to enable comparison between samples. The gradient length was quantified up to the threshold where the signal decreased to 20% of its maximum value (see Supplementary file 2). To test gradient length differences after silencing the proteomic candidates and the control, Pairwise Wilcoxon tests adjusted for multiple comparisons.

Labelling the endocytic and lysosomal compartment

To study the endocytic compartments, third instar larval discs were incubated in 3.7 mM Dextran (Dextran, Alexa FluorTM 647; 10,000 MW, Invitrogen) in the insect culture medium M3 medium at 25 °C for 10 min and then washed five times for 2 min prior to fixation in 4% paraformaldehyde with 0.05% Triton X-100 for 5 min at room temperature. The third instar larval discs were additionally incubated for 40 min at 25 °C with 100 nM lysotracker (LysoTrackerTM Red DND-99 Invitrogen), used for viable cell staining of lysosomes, before fixation in 4% paraformaldehyde with 0.05% Triton X-100. Dynasome (80 mM from Cayman Chemical Company), a cell-permeable small molecule that inhibits the GTPase activity of dynamin, was used prior to dextran incubation at 25 °C for 40 min.

Quantification of vesicle-like punctae

For quantification of vesicle-like punctae, we used the 'analyse particles' tool from Fiji (ImageJ) using a fluorescence threshold of 200–255 and counting of particles sized 5–20px. An automated macro script was designed and quantifications of 3 lateral sections were done in a selected window (266–182 px) located in the middle of the wing pouch. 8–10 discs per genotype were analysed and the averages per disc and treatment were then processed by ANOVA to obtain plots showing average and data variability.

Quantification of Cherio^{YFP}-Trap signal distribution

To determine Cher^{YFP}-Trap signal distribution, we used ImageJ analysis tools; the standard deviation parameter from plugins-integral image filters-standard deviation. This parameter considers the relationship of signal-covered area over its absence (black) in a selected window (580 × 175 px). Z-stacks were acquired from apical to basal (1 μ m interval) and a central lateral section was analysed per disc, measuring the experimental dorsal half and the ventral half as the internal control to obtain a ratio (dorsal/ventral) showing the proportion of change in the signal (protein) distribution. For modulation of endogenous Cher^{YFP} signal either by ectopic Ihog^{RFP} (or Ihog^{GFP}) or Ihog^{RNAi} expression, pairwise Wilcoxon tests adjusted for multiple comparisons were used.

Quantification of *Bac.hh^{SJGFP}* and *Bac.ihog^{GFP}* fluorescence ratio

To compare Ihog and Hh endogenous protein localization by different treatments dorsally and keeping the ventral half as an internal control of wild type condition, we applied Mean Gray Values from a fixed area (580 × 175 px) in each half of the disc. A ratio of potential change was obtained by dividing each dorsal value by its corresponding ventral value. Statistical analysis of rate values was done Pairwise Wilcoxon tests adjusted for multiple comparisons.

Quantification of cytoneme number and length

Cytoneme length and number were quantified within a selected window measuring 20% of the wing pouch size as described in ref. 6. Quantification for cytoneme number and length was done by comparing the control (UAS.Ihog^{RFP}) with the expression of Ihog^{RFP} after RNAi treatments for EGFR, Spitz, Vein and Cheerio, as well as Ihog^{RFP} expression and co-expression of the constitutively active EGFR, or the dominant negative forms of EGFR.

Quantification of cytoneme length and number reported by GMA^{GFP} expression after treatment with EGFR^{RNAi}, Ras1^{RNAi}, Ras1^{V12} and Ras1^{DN} were obtained using ImageJ software and the average length of the two longest cytonemes was used for the analysis with Pairwise Wilcoxon tests adjusted for multiple comparisons.

Protein isolation for mass spectrometry

We modified a standard protocol for immunoprecipitation using *Drosophila* embryos^{20,79}. Larvae expressing UAS.Ihog^{RFP} or UAS^{RFP} under *act.Gal4*, Gal80^{TS} for 18 h were collected and flash frozen in liquid Nitrogen and were homogenized in 2 ml/each of C Buffer (50 mM HEPES [pH7.4], 50 mM KCl, 1 mM MgCl, 1 mM EGTA, 0.1% Triton X-100, Protease inhibitors cocktail (Roche)). Extracts were initially clarified by centrifugation at 13,000 × *g* for 10 min, followed by two high-speed centrifugations at 120,000 × *g* for 10 min and 30 min. The supernatant was incubated with RFP-Trap coupled to agarose beads (Chromotek) for 1 h at 4 °C, then washed (5X with 15 min incubation periods) with C Buffer. Mass Spectrometry (MS) samples were then flash-frozen at −80 °C.

MS sequencing and basic analysis were performed at the Proteomics Facility of the University of Bristol. Samples were briefly run in an SDS-PA gel, cut as a single slice and subjected to in-gel tryptic digestion using a DigestPro automated digestion unit (Intavis Ltd). The resulting peptides were fractionated using a Dionex Ultimate 3000

nanoHPLC system in line with an LTQ-Orbitrap Velos mass spectrometer (Thermo Scientific). In brief, peptides in 1% (vol/vol) formic acid were injected onto an Acclaim PepMap C18 nano-trap column (Dionex). After washing with 0.5% (vol/vol) acetonitrile 0.1% (vol/vol) formic acid peptides were resolved on a 250 mm × 75 µm Acclaim PepMap C18 reverse phase analytical column (Dionex) over a 150 min organic gradient, using 7 gradient segments (1–6% solvent B) over 1 min, 6–15% B over 58 min, 15–32% B over 58 min, 32–40% B over 3 min, 40–90% B over 1 min, held at 90% B for 6 min and then reduced to 1% B over 1 min) with a flow rate of 300 nl min⁻¹. Solvent A was 0.1% formic acid and Solvent B was aqueous 80% acetonitrile in 0.1% formic acid. Peptides were ionized by nano-electrospray ionization at 2.1 kV using a stainless-steel emitter with an internal diameter of 30 µm (Thermo Scientific) and a capillary temperature of 250 °C.

Tandem mass spectra were acquired using an LTQ-Orbitrap Velos mass spectrometer controlled by Xcalibur 2.1 software (Thermo Scientific) and operated in data-dependent acquisition mode. The Orbitrap was set to analyse the survey scans at 60,000 resolution (at m/z 400) in the mass range m/z 300 to 2000 and the top twenty multiply charged ions in each duty cycle selected for MS/MS in the LTQ linear ion trap. Charge state filtering, where unassigned precursor ions were not selected for fragmentation, and dynamic exclusion (repeat count, 1; repeat duration, 30 s; exclusion list size, 500) was used. Fragmentation conditions in the LTQ were as follows: normalized collision energy, 40%; activation q, 0.25; activation time, 10 min; and minimum ion selection intensity, 500 counts.

The raw data files were processed and quantified using Proteome Discoverer software v1.2 (Thermo Scientific) and searched against the dmel-all-translation-r5.47 database using the SEQUEST (Ver. 28 Rev. 13) algorithm. Peptide precursor mass tolerance was set at 10 ppm, and MS/MS tolerance was set at 0.8 Da. Search criteria included carbamidomethylation of cysteine (+57.0214) as a fixed modification and oxidation of methionine (+15.9949) as a variable modification. Searches were performed with full tryptic digestion and a maximum of 1 missed cleavage was allowed. The reverse database search option was enabled, and all peptide data was filtered to satisfy false discovery rate (FDR) of 5%.

MS results were filtered by removing protein IDs with single peptide hits. We have produced a database of MS data accumulated from two independent Ihog^{RFP} expression experiments (Supplementary Data 1) and using extracts from larvae expressing RFP (i.e. negative control) (Supplementary Data 2). A spreadsheet incorporating these data was used to produce a list of false-positive protein IDs and their associated highest overall MS Area. Filtered Ihog^{RFP} results were cross-referenced against this database. Any protein ID that was either not identified in negative control list or was identified in negative controls with MS Scores of at least 10-fold less than in Ihog^{RFP} was kept, while all other protein IDs were discarded (Supplementary Data 3).

Co-immunoprecipitation assay

Immunoprecipitation was performed as above from larvae co-expressing Ihog^{RFP} and Cher^{YFP} (expressed at endogenous levels) or expressing RFP alone as control under *act.Gal4* (100 frozen larvae per genotype). Homogenized and clarified samples were also incubated with RFP-Trap coupled to agarose beads (Chromotek) for 1 h at 4 °C, then washed (5X) with C Buffer. To check for co-immunoprecipitation, samples were resuspended in sample buffer with B-mercaptoethanol and subjected to 1 D SDS-Page (6–15% gradient) and Western blotting. Blotted membranes were probed with appropriate antibodies, either to GFP (1:1000 mouse monoclonal Roche) or to RFP (rabbit polyclonal 1:5000 Abcam). Blots were incubated with fluorescent α-mouse (800CW) and α-rabbit (680RD) secondary antibodies (Li-Cor) and imaged with the 364-Odyssey equipment. Presentation of full scan blots seen in the source data file.

Reporting summary

Further information on research design is available in the Nature Portfolio Reporting Summary linked to this article.

Data availability

The mass spectrometry proteomics data have been deposited to the ProteomeXchange Consortium via the PRIDE [1] partner repository with the dataset identifier [PXD040793](https://doi.org/10.1038/s41467-025-57162-5). The remaining data are available within the article, Supplementary information or Source Data File. Source data is provided by this article. Source data are provided with this paper.

Code availability

The Matlab script used in this work is available as Supplementary Codes 1 and 2.

References

- Kornberg, T. B. Distributing signaling proteins in space and time: the province of cytonemes. *Curr. Opin. Genet. Dev.* **45**, 22–27 (2017).
- Kornberg, T. B. & Roy, S. Communicating by touch—neurons are not alone. *Trends Cell Biol.* **24**, 370–376 (2014).
- González-Méndez, L., Gradilla, A.-C. & Guerrero, I. The cytoneme connection: direct long-distance signal transfer during development. *Development* **146**, dev174607 (2019).
- Routledge, D. & Scholpp, S. Mechanisms of intercellular wnt transport. *Development* **146**, dev176073 (2019).
- Rojas-Ríos, P., Guerrero, I. & González-Reyes, A. Cytoneme-mediated delivery of Hedgehog regulates the expression of bone morphogenetic proteins to maintain germline stem cells in *Drosophila*. *PLoS Biol.* **10**, e1001298 (2012).
- Bischoff, M. et al. Cytonemes are required for the establishment of a normal Hedgehog morphogen gradient in *Drosophila* epithelia. *Nat. Cell Biol.* **15**, 1269–1281 (2013).
- Chen, W., Huang, H., Hatori, R. & Kornberg, T. B. Essential basal cytonemes take up hedgehog in the *Drosophila* wing imaginal disc. *Development* **144**, 3134–3144 (2017).
- González-Méndez, L., Seijo-Barandiará, I. & Guerrero, I. Cytoneme-mediated cell-cell contacts for Hedgehog reception. <https://doi.org/10.7554/eLife.24045.001> (2017)
- Sanders, T. A., Llagostera, E. & Barna, M. Specialized filopodia direct long-range transport of SHH during vertebrate tissue patterning. *Nature* **497**, 628–632 (2013).
- Zhang, Z. et al. Optogenetic manipulation of cellular communication using engineered myosin motors. *Nat. Cell Biol.* **23**, 198–208 (2021).
- Cardozo, M. J. et al. Cdon acts as a Hedgehog decoy receptor during proximal-distal patterning of the optic vesicle. *Nat. Commun.* **5**, 4272 (2014).
- Hall, E. T. et al. Cytoneme signaling provides essential contributions to mammalian tissue patterning. *Cell* **187**, 276–293.e23 (2024).
- Hall, E. T. et al. Cytoneme delivery of sonic hedgehog from ligand-producing cells requires myosin 10 and a dispatched-boc/cdon co-receptor complex. *eLife* **10**, 1–68 (2021).
- Aguirre-Tamaral, A. & Guerrero, I. Improving the understanding of cytoneme-mediated morphogen gradients by in silico modeling. *PLoS Comput. Biol.* **17**, e1009245 (2021).
- González-Méndez, L. et al. Polarized sorting of patched enables cytoneme-mediated Hedgehog reception in the *Drosophila* wing disc. *EMBO J.* **39**, e103629 (2020).
- Mattila, P. K. & Lappalainen, P. Filopodia: molecular architecture and cellular functions. *Nat. Rev. Mol. Cell Biol.* **9**, 446–454 (2008).
- Nobes, C. D. & Hall, A. Rho, Rac, and Cdc42 GTPases regulate the assembly of multimolecular focal complexes associated with actin stress fibers, lamellipodia, and filopodia. *Cell* **81**, 53–62 (1995).
- Fischer, R. S., Lam, P. Y., Huttenlocher, A. & Waterman, C. M. Filopodia and focal adhesions: An integrated system driving branching

- morphogenesis in neuronal pathfinding and angiogenesis. *Dev. Biol.* **451**, 86–95 (2019).
19. Jacquemet, G., Hamidi, H. & Ivaska, J. Filopodia in cell adhesion, 3D migration and cancer cell invasion. *Curr. Opin. Cell Biol.* **36**, 23–31 (2015).
 20. Antrobus, R. & Wakefield, J. G. Isolation, identification and validation of microtubule associated proteins from drosophila embryos. *Methods Mol. Biol.* **777**, 273–292 (2011).
 21. Simon, E. et al. Glypicans define unique roles for the Hedgehog co-receptors Boi and Ihog in cytoneme-mediated gradient formation. *eLife* **10**, e64581 (2021).
 22. Yao, S., Lum, L. & Beachy, P. The Ihog cell-surface proteins bind hedgehog and mediate pathway activation. *Cell* **125**, 343–357 (2006).
 23. Aguirre-Tamaral, A., Cambón, M., Poyato, D., Soler, J. & Guerrero, I. Predictive model for cytoneme guidance in Hedgehog signaling based on Ihog- Glypicans interaction. *Nat. Commun.* **13**, 5647 (2022).
 24. Yang, S. et al. Competitive coordination of the dual roles of the hedgehog co-receptor in homophilic adhesion and signal reception. *eLife* **10**, e65770 (2021).
 25. Jiang, X. et al. Inhibition of Cdc42 is essential for Mig-6 suppression of cell migration induced by EGF. www.impactjournals.com/oncotarget (2016).
 26. Kyriakopoulou, K. et al. EGFR/ERβ-mediated cell morphology and invasion capacity are associated with matrix culture substrates in breast cancer. *Cells* **9**, 2256 (2020).
 27. Rijken, P. J., Hage, W. J., Van Bergen En Henegouwen, P. M. P., Verkleij, A. J. & Boonstra, J. Epidermal growth factor induces rapid reorganization of the actin microfilament system in human A431 cells. *J. Cell Sci.* **100**, 491–499 (1991).
 28. Song, W., Xuan, H. & Lin, Q. Epidermal growth factor induces changes of interaction between epidermal growth factor receptor and actin in intact cells. *Acta Biochim. Biophys. Sin.* **40**, 754–760 (2008).
 29. Yasui, H., Ohnishi, Y., Nakajima, M. & Nozaki, M. Migration of oral squamous cell carcinoma cells are induced by HGF/c-Met signaling via lamellipodia and filopodia formation. *Oncol. Rep.* **37**, 3674–3680 (2017).
 30. Maisel, S., Broka, D. & Schroeder, J. Intravesicular epidermal growth factor receptor subject to retrograde trafficking drives epidermal growth factor-dependent migration. *Oncotarget* **9**, 6463–6477, www.impactjournals.com/oncotarget (2018).
 31. Zschätzsch, M. et al. Regulation of branching dynamics by axon-intrinsic asymmetries in tyrosine kinase receptor signaling. *eLife* **3**, e01699 (2014).
 32. Peng, Y., Han, C. & Axelrod, J. D. Planar polarized protrusions break the symmetry of EGFR signaling during drosophila bract cell fate induction. *Dev. Cell* **23**, 507–518 (2012).
 33. Pan, W. et al. Oncogenic BRAF noncanonically promotes tumor metastasis by mediating VASP phosphorylation and filopodia formation. *Oncogene* **42**, 3194–3205 (2023).
 34. Gonzalez, C. Drosophila melanogaster: a model and a tool to investigate malignancy and identify new therapeutics. *Nat. Rev. Cancer* **13**, 172–183 (2013).
 35. Ninov, N., Manjón, C. & Martín-Blanco, E. Dynamic control of cell cycle and growth coupling by ecdysone, egfr, and PI3K signaling in Drosophila histoblasts. *PLoS Biol.* **7**, 0892–0903 (2009).
 36. Freeman, M. Complexity of EGF receptor signalling revealed in drosophila. *Curr. Opin. Genet. Dev.* **8**, 407–411 (1998).
 37. Brown, K. E., Kerr, M. & Freeman, M. The EGFR ligands Spitz and Keren act cooperatively in the Drosophila eye. *Dev. Biol.* **307**, 105–113 (2007).
 38. Schnepf, B., Grumblin, G., Donaldson, T. & Simcox, A. Vein is a novel component in the Drosophila epidermal growth factor receptor pathway with similarity to the neuregulins. *Genes Dev.* **10**, 2302–2313 (1996).
 39. Miura, G. I. et al. Palmitoylation of the EGFR ligand spitz by rasp increases spitz activity by restricting its diffusion. *Dev. Cell* **10**, 167–176 (2006).
 40. Simcox, A. Differential requirement for EGF-like ligands in Drosophila wing development. *Mech. Dev.* **62**, 41–50 (1997).
 41. Klämbt, C. EGF receptor signalling: the importance of presentation activation of the Drosophila EGF receptor requires the transmembrane TGF-α-like ligand spitz. recent studies have shed new light on the role of two transmembrane proteins, star and rhomboid, in the presentation and subsequent proteolytic processing of Spitz. *Curr. Biol.* **10**, 388–391 (2000).
 42. Tsruya, R. et al. Intracellular trafficking by star regulates cleavage of the Drosophila EGF receptor ligand Spitz. *Genes Dev.* **16**, 222–234 (2002).
 43. Crozatier, M., Glise, B. & Vincent, A. Connecting Hh, Dpp and EGF signalling in patterning of the Drosophila wing; the pivotal role of collier/knot in the AP organiser. *Development* **129**, 4261–4269 (2002).
 44. Zheng, X., Mann, R. K., Sever, N. & Beachy, P. A. Genetic and biochemical definition of the Hedgehog receptor. *Genes Dev.* **24**, 57–71 (2010).
 45. Hsia, E. Y. C. et al. Hedgehog mediated degradation of Ihog adhesion proteins modulates cell segregation in Drosophila wing imaginal discs. *Nat. Commun.* **8**, 1275 (2017).
 46. Yan, D. et al. The cell-surface proteins Dally-like and Ihog differentially regulate Hedgehog signaling strength and range during development. *Development* **137**, 2033–2044 (2010).
 47. Bilioni, A. et al. Balancing Hedgehog, a retention and release equilibrium given by Dally, Ihog, Boi and shifted/DmWif. *Dev. Biol.* **376**, 198–212 (2013).
 48. Wu, X. et al. The Drosophila Hedgehog receptor component Interference hedgehog (Ihog) mediates cell–cell interactions through trans-homophilic binding. *J. Biol. Chem.* **294**, 12339–12348 (2019).
 49. Buszczak, M. et al. The carnegie protein trap library: a versatile tool for drosophila developmental studies. *Genetics* **175**, 1505–1531 (2007).
 50. Lye, C. M., Naylor, H. W. & Sanson, B. Subcellular localisations of the CPTI collection of YFP-tagged proteins in Drosophila embryos. *Development* **141**, 4006–4017 (2014).
 51. Külshammer, E. & Uhlirova, M. The actin cross-linker Filamin/Cheerio mediates tumor malignancy downstream of JNK signaling. *J. Cell Sci.* **126**, 927–938 (2013).
 52. Külshammer, E. et al. The mechanosensor Filamin A/Cheerio promotes tumorigenesis via specific interactions with components of the cell cortex. *FEBS J.* **289**, 4497–4517 (2022).
 53. Kim, S. et al. Graf regulates hematopoiesis through GEEC endocytosis of EGFR. *Development* **144**, 4159–4172 (2017).
 54. Callejo, A. et al. Dispatched mediates Hedgehog basolateral release to form the long-range morphogenetic gradient in the Drosophila wing disk epithelium. *Proc. Natl Acad. Sci. USA* **108**, 12591–12598 (2011).
 55. Qi, Y. et al. Ihog proteins contribute to integrin-mediated focal adhesions. *Sci. China Life Sci.* **66**, 366–375 (2022).
 56. Fereres, S., Hatori, R., Hatori, M. & Kornberg, T. B. Cytoneme-mediated signaling essential for tumorigenesis. *PLoS Genet.* **15**, e1008415 (2019).
 57. Mattes, B. et al. Wnt/PCP controls spreading of Wnt/b-catenin signals by cytonemes in vertebrates. *Elife* **7**, e36953 (2018).
 58. Pinto, G., Brou, C. & Zurzolo, C. Tunneling nanotubes: the fuel of tumor progression? *Trends Cancer* **6**, 874–888 (2020).
 59. Portela, M. Tumorigenesis: using cytonemes to engage mesenchymal cells in epithelial tumours. *Curr. Biol.* **30**, R441–R443 (2020).
 60. Rogers, S. et al. Cancer-associated fibroblasts influence Wnt/PCP signaling in gastric cancer cells by cytoneme-based dissemination of ROR2. *Proc. Natl Acad. Sci. USA* **120**, e2217612120 (2023).

61. Routledge, D. et al. The scaffolding protein flot2 promotes cytoneme-based transport of wnt3 in gastric cancer. *eLife* **11**, e77376 (2022).
62. Prober, D. A. & Edgar, B. A. Ras1 promotes cellular growth in the drosophila wing cycle in *saccharomyces cerevisiae*, where activation of the Ras/cAMP pathway by improved nutrient conditions increases cell size (reviewed by Thevelein and de Winder. *Cell* **100**, 435–446 (2000).
63. Amin, A., Li, Y. & Finkelstein, R. Hedgehog activates the EGF receptor pathway during *Drosophila* head development. *Development* **126**, 2623–2630 (1999).
64. Aberger, F. & Ruiz i Altaba, A. Context-dependent signal integration by the GLI code: the oncogenic load, pathways, modifiers and implications for cancer therapy. *Semin. Cell Dev. Biol.* **33**, 93–104 (2014).
65. Götschel, F. et al. Synergism between Hedgehog-GLI and EGFR signaling in Hedgehog-responsive human medulloblastoma cells induces downregulation of canonical Hedgehog-target genes and stabilized expression of GLI1. *PLoS ONE* **8**, e65403 (2013).
66. Özkan, E. et al. An extracellular interactome of immunoglobulin and LRR proteins reveals receptor-ligand networks. *Cell* **154**, 228–239 (2013).
67. Yagi, R., Mayer, F. & Basler, K. Refined LexA transactivators and their use in combination with the *Drosophila* Gal4 system. *Proc. Natl Acad. Sci. USA* **107**, 16166–16171 (2010).
68. Calleja, M., Moreno, E., Pelaz, S. & Morata, G. Visualization of gene expression in living adult *Drosophila*. *Science* **274**, 252–255 (1996).
69. Tanimoto, H., Itoh, S., ten Dijke, P. & Tabata, T. Hedgehog creates a gradient of DPP activity in *Drosophila* wing imaginal discs. *Mol. Cell* **5**, 59–71 (2000).
70. Hinz, U., Giebel, B. & Campos-Ortega, J. A. The basic-helix-loop-helix domain of *Drosophila* lethal of scute protein is sufficient for proneural function and activates neurogenic genes. *Cell* **76**, 77–87 (1994).
71. Bloor, J. W. & Kiehart, D. P. Zipper nonmuscle myosin-II functions downstream of PS2 integrin in *Drosophila* myogenesis and is necessary for myofibril formation. *Dev. Biol.* **239**, 215–228 (2001).
72. Karim, F. D. & Rubin Gerald, M. Ectopic expression of activated Ras1 induces hyperplastic growth and increased cell death in *Drosophila* imaginal tissues. *Development* **125**, 1–9 (1998).
73. Siegrist, S. E., Haque, N. S., Chen, C. H., Hay, B. A. & Hariharan, I. K. Inactivation of both Foxo and reaper promotes long-term adult neurogenesis in *Drosophila*. *Curr. Biol.* **20**, 643–648 (2010).
74. Nir, R., Grossman, R., Paroush, Z. & Volk, T. Phosphorylation of the *drosophila* melanogaster RNA-binding protein how by MAPK/ERK enhances its dimerization and activity. *PLoS Genet.* **8**, e1002632 (2012).
75. Schweitzer, R., Howest, R., Smith, R., Shllo, B.-Z. & Matthew Freeman, B. Inhibition of *Drosophila* EGF receptor activation by the secreted protein Argos. *Nature* **376**, 699–702 (1995).
76. Capdevila, J. et al. The *Drosophila* segment polarity gene patched interacts with decapentaplegic in wing development. *EMBO J.* **1**, 71–82 (1994).
77. R Development Core Team. 2019 R Core Team. A language and environment for statistical computing. *R Foundation for Statistical Computing*, Vienna, Austria. URL <https://www.R-project.org/>. R Foundation for Statistical Computing. (2020).
78. Mathworks Inc. MATLAB and statistic toolbox release. www.mathworks.com/products/matlab (2016).
79. Palumbo, V. et al. Misato controls mitotic microtubule generation by stabilizing the TCP-1 tubulin chaperone complex [corrected]. *Curr. Biol.* **25**, 1777–1783 (2015).

Acknowledgements

We are grateful to Pedro Ripoll, Gustavo Aguilar and Nicole Gorfinkiel for comments on the manuscript and to Lara Rodenstein for her excellent technical assistance. We are also thankful to P. Beachy, J. Treisman, R. Holgreen, T. Tabata, A. Simcox and T. Kornberg for stocks and reagents and to the Proteomic Facility of the University of Bristol, specially to Kate Heesom, for their kind services towards proteomics analysis. Finally, AAT acknowledges the support of the field of excellence ‘Complexity of life in basic research and innovation’ of the University of Graz. Work was supported by grants from the Spanish Ministry of Science, Innovation and Universities grants to IG: BFU2017-83789-P with fellowships PRI 2018-085510 for C.J.-J., FJCI-2014-19819 to S.J.-A and PID2020-114533GB-C21 with a fellowship PRI 2021-097741 for C.F.-P., fellowship PEJD-2018-PRE/BMD-8988 from Comunidad de Madrid to I.S.-P and grant to A.-C.G.: BFU2015-73609-JIN, by grant BBSRC to J.G.W.: BB/K017837/1 and by institutional grants from the Fundación Areces and from Banco de Santander to the CBMSO.

Author contributions

Conception of the project by A.-C.G. and I.G.; A.-C.G., V.S.L. and I.G. designed the research, V.S.L., A.-C.G., C.J.-J., C.F.-P., D.S.-H., and I.S.-P. performed research; A.-C.G., V.S.L., A.A.-T., J.G.W. and I.G. analyzed the data, and A.-C.G., V.S.L. and I.G. wrote the paper.

Competing interests

The authors declare no competing interests.

Additional information

Supplementary information The online version contains supplementary material available at <https://doi.org/10.1038/s41467-025-57162-5>.

Correspondence and requests for materials should be addressed to Isabel Guerrero.

Peer review information *Nature Communications* thanks Raghuveera Goel and the other, anonymous, reviewer(s) for their contribution to the peer review of this work. A peer review file is available.

Reprints and permissions information is available at <http://www.nature.com/reprints>

Publisher’s note Springer Nature remains neutral with regard to jurisdictional claims in published maps and institutional affiliations.

Open Access This article is licensed under a Creative Commons Attribution-NonCommercial-NoDerivatives 4.0 International License, which permits any non-commercial use, sharing, distribution and reproduction in any medium or format, as long as you give appropriate credit to the original author(s) and the source, provide a link to the Creative Commons licence, and indicate if you modified the licensed material. You do not have permission under this licence to share adapted material derived from this article or parts of it. The images or other third party material in this article are included in the article’s Creative Commons licence, unless indicated otherwise in a credit line to the material. If material is not included in the article’s Creative Commons licence and your intended use is not permitted by statutory regulation or exceeds the permitted use, you will need to obtain permission directly from the copyright holder. To view a copy of this licence, visit <http://creativecommons.org/licenses/by-nc-nd/4.0/>.

© The Author(s) 2025